bushfire CRC

UNDERSTANDING COMPLEX FIRE BEHAVIOUR: MODELLING INVESTIGATION OF LOFTING PHENOMENA AND WIND VARIABILITY

FINAL REPORT FOR THE LOFTING PHENOMENA AND WIND VARIABILITY PROJECT

William Thurston, Robert J. B. Fawcett, Kevin J. Tory and Jeffrey D. Kepert

The Centre for Australian Weather and Climate Research, Bureau of Meteorology

Australian Government
Bureau of Meteorology

Publisher: Bushfire Cooperative Research Centre, East Melbourne, Victoria

Cover:
Smoke plume from the Tostaree bushfire in Victoria, February 2011.
Photo by Gail Wright, Department of Environment and Primary Industries.

ISBN: 978-0-9875218-8-0

Citation:
Thurston W, Fawcett RJB, Tory KJ, Kepert JD, (2014) Understanding Complex Fire Behaviour: Modelling Investigation of Lofting Phenomena and Wind Variability, Bushfire CRC, Australia, ISBN: 978-0-9875218-8-0

Contents

Executive Summary

This project investigates two meteorological contributions to complex fire behaviour: (i) wind direction variability, known to broaden fire fronts leading to more rapid fire propagation, and (ii) wind influence on fire plume structure, with emphasis on firebrand lofting potential.

State of knowledge:

Prior to the commencement of this project, wind variability associated with the turbulent atmospheric boundary layer (length scales less than about 100 m) was well understood, as was larger-scale wind variability associated with synoptic and mesoscale weather phenomena (length scales > 10 km). A knowledge gap existed in the scales in between. One meteorological phenomenon that sits in this knowledge gap is boundary-layer rolls, which are known to produce large wind direction variability, and they were present during the Black Saturday bushfires. For this reason we chose to devote a large proportion of the project to investigating boundary-layer rolls. Prior to this project, studies had documented extensively the conditions in which boundary-layer rolls form, their structure and their impact on a range of phenomena such as thunderstorm formation, dust dispersion and air quality. Despite being a well-studied phenomenon, little was known about their potential impacts on bushfire behaviour, apart from one modelling study that demonstrated fire spread was enhanced by the presence of boundary-layer rolls. Furthermore, boundary-layer roll modelling studies were limited to idealised large-eddy simulations: they had never been investigated in numerical weather prediction models.

Perhaps surprisingly the wind influence on fire plume structure is not well understood, with only qualitative relationships between some wind regimes and plume structure having been identified in observational and modelling studies. A quantitative relationship has been elusive due to observational difficulties and the very wide range of potential plume structures and behaviours associated with a seemingly infinite range of possible wind and atmospheric

stability regimes. This is further complicated by additional variables such as humidity, terrain and fuel types. An early theoretical study attempted to quantify plume behaviour based on a simple energetics argument that pitted plume energy against wind energy to separate the plume into one of two categories. Subsequent field studies have failed to support the theory, perhaps because the model was too simplistic. In recent times, computing power has enabled realistic plume modelling and the potential to perform hundreds or even thousands of simulations to establish a plume structure and behaviour climatology as a function of background wind. However, prior to this CRC project very few plume simulations had been performed. Of these prior simulations, none have focused on lofting potential, and none have been performed in what we believe to be a realistic turbulent boundary layer. This field of research is very young and provides a great opportunity to do highly valuable work for fire management applications relating to understanding fire behaviour.

Progression of research:

In the first year of the study the research focused on the boundary-layer rolls investigation, using the Bureau of Meteorology's operational forecast system (ACCESS) in hindcast mode, run at very high resolution (grid spacing of about 440 m). The research benefitted from shared skills, tools and expertise in another Bushfire CRC project (FireDST), and used one of the simulations from that project, which enabled a rapid spin-up for this project. The FireDST project also benefitted from shared data analysis. It soon became apparent that ACCESS was not the ideal system for investigating fire plume behaviour. Thus, for the second part of the project, considerable effort was invested to identify, obtain, install and learn to use the best tool available to us for the job: the UK Met Office Large-Eddy Model (LEM). This model proved to be excellent for this purpose: it is versatile and produces very realistic turbulence, which is particularly important for plume studies. While the LEM does not specifically model fire occurrence, an intense surface heat source was added to simulate the heat from a fire, using a technique from previous plume studies. As this project focusses

on dry atmospheric processes, no moisture release from combustion is parameterised. Moist processes will be included in the future in order to model pyrocumulus plumes. The model atmosphere responds by generating updraft plumes, with very realistic behaviour. Later in the project a uniform surface heat flux was introduced to the LEM in a high-wind environment (similar to Black Saturday) in order to initiate boundary-layer rolls. This and similar simulations were used to study plume behaviour in ascending and descending branches of the rolls. An ember-tracking algorithm was developed with the view to trace hypothetical embers lofted by the plume of varying fall speeds in order to improve understanding of ember dispersion under a variety of wind regimes. This aspect of the work is currently ongoing.

Research results:

Boundary-layer rolls

The boundary-layer rolls formed when the model simulated solar heating warmed the land surface, creating an instability (specifically, warmer surface air overlayed by cooler air). The instability was released by an overturning circulation. The specific wind and surface heating regime led to the organisation of the ascending and descending regions into lines approximately parallel with the wind that make up pairs of counter-rotating gyres or rolls that rotate with a horizontal axis. This circulation pattern carries warm surface air to the top of the boundary layer (typically 1 to 2 km deep, but close to 5 km deep on Black Saturday) and brings relatively cooler air to the surface. At the surface, the air converges inwards towards the ascending regions, and diverges outwards from the descending regions, giving rise to a 30° deviation each way from the average direction of the mean wind.

The following important potential impacts of boundary-layer rolls on fire spread were identified in the Black Saturday simulation.

i) Wind direction variability: With respect to a given surface location, the rolls meander and propagate laterally (i.e., with a component perpendicular to the mean wind direction), bringing surface winds that back and veer through 60 degrees with alternating passage of updraft and downdrafts overhead.

ii) Firebrand lofting: The maximum updraft speed in the simulated Black Saturday boundary-layer rolls was in excess of 8 m s^{-1} at about 2 km above the surface. It is conceivable that such an updraft passing over a fire could loft embers and firebrands already raised by the fire plume even higher, facilitating long-range spotting.

iii) Enhanced FFDI: The Forest Fire Danger Index (FFDI) was found to be highest beneath the descending branches of the boundary-layer rolls, where the surface wind speeds were greatest. This is despite the temperature being highest below the updrafts. This is perhaps the intuitive expectation, given that severe fire weather conditions as represented by indices such as the FFDI are typically more dependent on the occurrence of high wind speeds than high temperatures. The relative humidity varied very little. Later in the day the boundary-layer rolls began to break down, the convection became more cellular, and the downdrafts became more concentrated and intense. The maximum horizontal wind speed increased as a down-burst like flow pattern began to develop, leading to small patches of even higher FFDI. (Divergence of the downward flow as it impacted the surface accelerated the winds on the downwind side of the downburst.)

iv) Pyrocumulus development: While there was no evidence of pyrocumulus activity in the ACCESS simulations (because there is no fire in the model), the strong updrafts evident in the boundary-layer rolls could trigger deep pyrocumulus activity in the real world. The updrafts in boundary-layer rolls have been known to trigger cumulonimbus clouds and thunderstorm development. Thus, it is conceivable that the heat and moisture from a fire plume lofted further in a

boundary-layer roll updraft could also trigger cloud development, including intense pyrocumulus activity.

Plume lofting results

As this area of research is still in its infancy, perhaps the most important outcome of this work was the development and validation of a realistic framework with which useful plume experiments can be performed. As noted above, the model was integrated forward in time for several hours until a realistic turbulent wind structure developed: following this, the plume was initiated using a surface heat source. Inspection of this pre-plume wind structure revealed realistic turbulence structures and a realistic vertical profile of the mean wind (i.e., the well-observed logarithmic wind profile and profiles of turbulence statistics). Given that plume behaviour is sensitive to the background wind environment, it was important to reproduce these structures.

Because the atmospheric parameter space alone is considerable, with any number of wind and thermodynamic profile combinations possible, it was decided that a systematic approach would be taken using the simplest set of realistic scenarios, in which a constant initial background wind speed was applied to each experiment. The background wind speeds were 2, 5, 7.5, 10, 12.5 and 15 m s^{-1}. Parameters held constant included: flat terrain, a dry atmosphere, a thermodynamically neutral boundary layer 3 km deep, with typical tropospheric stability above, and a circular heat source of 250 m radius and an intensity of 100 kW m^{-2}.

The plumes that developed in the lower wind-speed environments tended to be taller and have stronger updrafts that were nearly laminar throughout much of the plume, with turbulent

characteristics only in the upper regions, whereas for the higher wind-speed environments the plumes were bent over and turbulent virtually from the surface upwards. With increasing wind-speeds over the heat source the plume was advected further downwind, and became more “puff-like” (i.e., containing intermittent, isolated puffs of rising hot air). Maximum updraft speeds were much higher in the laminar parts of the plumes than in the turbulent parts. Turbulence enhances the entrainment of cooler environmental air, which mixes with and dilutes the warmer plume, thereby reducing the plume buoyancy, updraft speeds and plume depth.

Despite a wide variation in plume structure across the wind speed regimes, all plumes showed considerable potential for firebrand lofting. A simple argument for estimating downstream firebrand transport revealed that the greatest downstream transport occurred for one of the intermediate background wind speeds, due to the optimum balance between time spent falling (associated with the lofting depth), and the time taken for advection downstream. In reality a broad distribution of firebrand transport from each plume would be expected. A Lagrangian transport model is currently under construction to calculate a more realistic firebrand transport distribution.

The other wind versus plume relationship investigated in this study yielded surprising and very important results. By simulating boundary-layer rolls with the LEM, an investigation into plume structure and behaviour in an environment of ascent and descent was made possible. Plumes located in the ascending branches of the boundary-layer rolls were considerably more intense, more spatially compact, and significantly deeper than plumes in the descent region compared with the same scenario without boundary-layer rolls. Furthermore, plumes in the descent region were even shallower, more horizontally spread out, and more puff-like, even though the parameterised fire size and intensity was the same. As the boundary-layer

rolls meandered and propagated across the domain, the plumes encountered alternating regions of ascent and descent, which led to rapid transitions between enhanced and suppressed plume behaviour.

Based on the simple arguments above it would be expected that plumes located in the ascending branches of the boundary-layer rolls would have significantly greater potential for firebrand lofting and downstream transport, and plumes in the descending branches would have relatively suppressed lofting potential. However, rapid changes in lofting potential might be expected over time-scales of tens of minutes.

As noted above, these experiments consider only the plume sensitivity to a very limited sample of wind scenarios. More complex wind scenarios of light winds near the surface and stronger winds aloft for example, could have greater potential for horizontal firebrand transport. The addition of moisture to the model, could further enhance lofting and horizontal transport potential if additional buoyancy were to be added to the plume through condensational heating, similar to pyrocumulus development. Plume depth will also vary with dry atmospheric stability and the intensity and size of the parameterised fire heat source. Plume sensitivity to these variables is an important topic for future work.

State of knowledge now:

Almost every result from the LEM studies has contributed to an advancement of the state of knowledge of plume behaviour in a realistic turbulent boundary layer. We now know that an intense heat source in a low-wind speed environment generates a deep, intense and coherent plume that can penetrate many kilometres into the stable layer above the well-mixed boundary layer, with updraft speeds in excess of 20 m s^{-1}. It follows that entrainment

into such a plume must be minimal for it to remain buoyant to such a great height. With increasing wind speeds, the plume becomes shallower, less intense, more bent over and increasingly more puff-like. The higher wind speeds advect the plume downwind, leading to the bent-over appearance. We expect the increasing energy of the turbulence in the higher wind cases to facilitate greater entrainment, which would reduce the plume buoyancy and also encourage the breakdown of the plume into buoyant puffs, leading to very realistic-looking bushfire-like smoke behaviour.

We now know that an intense circular heat source of 100 kW m^{-2} over a radius of 250 m will generate updraft speeds capable of lofting large firebrands (with fall velocities of up to 6 m s^{-1}) more than 1 km deep for all background wind speeds up to at least 15 m s^{-1}. Indeed, if a fire is capable of burning at that intensity in a background wind environment of 2 m s^{-1}, lofting to 6 km deep (in an environment of typical tropospheric stability) without any contribution to plume buoyancy from condensational heating seems quite plausible.

This project has revealed that plume behaviour in a strong background wind environment (15 m s^{-1}) can be particularly sensitive to environmental ascent and descent in the immediate vicinity of the plume. In a relatively weakly ascending region the plume becomes more upright, and very much more concentrated and coherent, with an almost doubling of the plume height. We suspect the more rapid ascent reduces the time for entrainment to dilute the plume buoyancy, and reduces the downstream plume advection and thus the tendency to break the plume into buoyant puffs. On the other hand the weaker, more bent-over and spread-out plumes in the descent regions, are advected further downstream which is likely to favour the plume break-down into buoyant puffs as the plume is stretched out horizontally. The greater surface area of the plume and puffs is expected to enhance entrainment of cooler environmental air, which will further dilute the plume and puff

buoyancy. If the plume and puff entrainment is governed to a large extent by the surface area and exposure time, we hypothesise a positive feedback in which a plume that is suppressed by environmental descent will spend more time entraining cooler environmental air. The greater buoyancy dilution rate will lead to a greater reduction in upward plume and puff acceleration, resulting in greater entrainment and plume and puff deceleration. The opposite will be true for a plume in a region of ascent. With respect to dangerous plume behaviour, these results suggest regions of ascent are likely to be particularly hazardous, because they contribute to firebrand lofting, and they strengthen the plume.

While this plume behaviour was identified in a simulation in which boundary-layer rolls provided the vertical flow, the lessons learned suggest any meteorological phenomena that produces local ascent should be of concern. This includes wind changes associated with trough lines, cold fronts, sea breezes, and solitary waves such as the undular bore observed during Black Saturday. It also includes the ascending branches of dry cellular convection, and especially moist convection. Pyrocumulus is potentially an extreme example when the moist ascent region can become attached to the plume itself. These conclusions are consistent with many studies and considerable anecdotal evidence of unexpected extreme fire behaviour.

The boundary-layer roll ACCESS modelling study largely confirmed suspected wind behaviour known to influence fire spread rates: horizontal wind direction variability, and ascent and descent associated with the vertical circulation. What was surprising was the large extent of the periodic wind direction variability (up to 60°) and the strength of the maximum updraft (> 8 m s^{-1}). These results together with the plume study suggest boundary-layer rolls could contribute to more destructive fire behaviour than previously thought, with the wind direction variability contributing to a broader and faster moving fire

front, and the updrafts contributing to enhanced lofting potential, and an intensification of the plume. Additionally, the greatest FFDI was found to be located in the descent region, which potentially could partly offset or override the effect of the suppressed plume found in regions of descent.

1 Introduction

This project investigates meteorological contributions to complex fire behaviour and rapid fire spread. The focus is on (i) wind direction variability, known to broaden fire fronts leading to more rapid fire propagation, and (ii) wind influence on fire plume structure, with emphasis on firebrand lofting potential.

1.1 Wind direction variability – Boundary-layer rolls

Wind direction variability in the boundary layer contributes to lateral fire spread by broadening the fire front. This broadening increases the front propagation speed, makes the fire more difficult to suppress and results in a larger area of damage. Wind direction variability on the turbulent (small) and synoptic (large) scales is relatively well understood. The spatial and temporal scales of wind direction variability which are relevant to fire spread are in the so-called 'spectral gap' (Stull, 1988) between the turbulent and synoptic scales. Sources of such wind direction variability at the surface include boundary-layer rolls (Etling and Brown 1993), convective clouds (Vincent et al. 2012), and topographically induced flows and meandering plumes (Mahrt 2011). During Black Saturday (7 February 2009) extensive cloud streets approximately aligned with the north-westerly airflow were visible in the satellite imagery, indicating the presence of boundary-layer rolls at a time when the Kilmore East fire was particularly intense (Figure 1.1, VBRC 2010).

One might expect the boundary-layer rolls to have had some, or perhaps even a significant, influence on the fire behaviour. For this reason Stage (i) of the project focusses on the boundary-layer rolls modelled in the Australian Community Climate and Earth-System Simulator (ACCESS) simulations of Black Saturday that were part of a related Bushfire CRC project: Fire Impact and Risk Evaluation Decision Support Tool (FireDST). These simulations were made possible by ongoing improvements in numerical weather prediction (NWP) and increasing computer power that has led to the ability to resolve features approaching 1 km in scale, and provide an unprecedented window

into atmospheric structures such as boundary-layer rolls that will likely affect fire behaviour. Since bushfire behaviour is sensitive to a very wide scale (both temporal and spatial) of atmospheric features it is important that numerical models used to study fire and fire weather adequately represent these features. This includes the large-scale and long-term climate (e.g., drought), through the medium-scale (weather systems such as fronts and wind changes) to the small-scale (short-term fluctuations in humidity and wind).

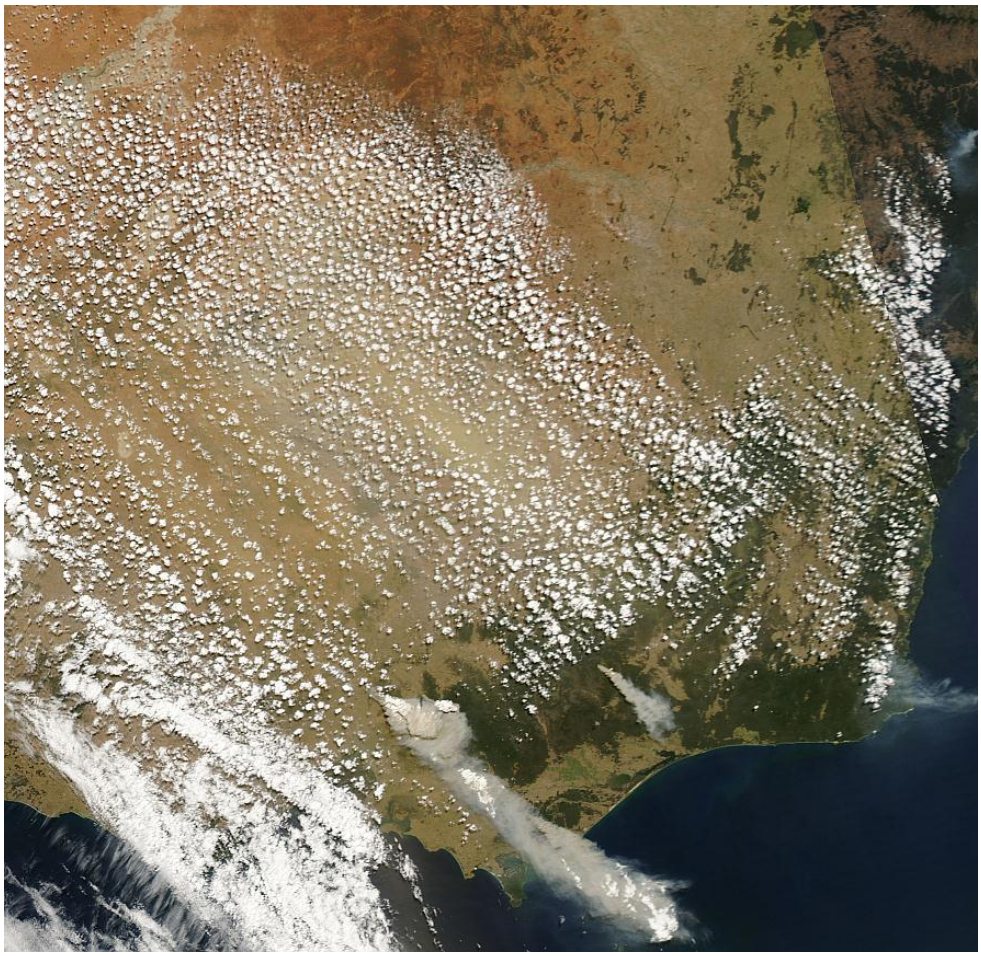

Figure 1.1: MODIS satellite image of south-eastern Australia during Black Saturday at about 0450 UTC (1550 EDT), when a wind change was located near the cloud band to the lower left of the image. The convective clouds ahead of the change are loosely organised into a quasi-linear pattern known as cloud streets, indicative of boundary-layer rolls.

1.2 Wind influence on plume structure

Stage (ii) of the project investigates conditions that lead to spot fires, which result in unpredictable fire behaviour and accelerated fire spread (e.g., Byram 1959). Spot fires develop when burning embers or firebrands are lofted into strong ambient winds. Anecdotal evidence suggests that this lofting and transport of firebrands can be responsible for the ignition of spot fires tens of kilometres ahead of the fire front (e.g., Cruz et al. 2012 reported evidence of 30 km spotting). Firebrand lofting occurs when updraft velocities exceed the terminal velocity of burning embers. Thus, the stronger, deeper and more sustained the vertical velocity, the higher firebrands can be lofted and the larger (denser) the firebrands that can be lofted. Updraft sources that can potentially facilitate firebrand lofting include,

1. Meteorological phenomena such as,
    - Mountain waves, rotors and associated terrain-induced circulations
    - Sea breezes, frontal passages and other convergence lines
    - Boundary-layer rolls, cellular convection and associated circulations
2. Smoke plumes (buoyant fire gases and smoke) in,
    - Conventional smoke plumes
    - Fire convective columns and associated pyro-convection, and pyro-tornadoes.

The smoke plumes are always collocated with the fire and ember source, whereas the listed meteorological phenomena, which are more spatially and temporally transient in nature, may only be briefly collocated with the fire. Furthermore, fire convective columns typically have near-surface updraft speeds greater than the meteorological phenomena, and thus have the greater potential for lofting. However, much anecdotal evidence exists to suggest the above meteorological phenomena interacting with fires can result in the transition from a conventional smoke plume with relatively weak updrafts to a fire convective column with likely intense updrafts. Anecdotal evidence also suggests the most intense updrafts are associated with rotating convective columns. These columns also have very deep updraft regions, further adding to their potential for firebrand lofting.

When firebrands are lofted to large heights above the fire from which they originate, they often travel faster and in a different direction from the near-surface winds, due to vertical wind shear. This means that fires spread by spotting can travel fast and be especially unpredictable. There is evidence of long-range spotting in excess of 30 km during the Black Saturday bushfires (e.g., Cruz et al. 2012). It is therefore desirable to have a good understanding of the dynamics of bushfire plumes and updrafts, in order to assess the potential for spotting and the associated dangerous fire spread.

Previous observational work has suggested that the interaction of the fire plume with the background wind is critical in determining the plume behaviour (e.g., Byram 1959), essentially through a balance between the potential energy of the buoyant plume and the kinetic energy of the winds. Attempts to fully address this idea have been hampered by a lack of good-quality observational datasets in consistent conditions that cover a wide-enough parameter space of wind and fire intensities.

Recently, computer power has increased to the point at which idealised meteorological models are able to be run at high-enough resolutions to explore the response of bushfire plumes to different background winds. However, often they have been used in a two-dimensional configuration or without spinning up a turbulent atmospheric boundary layer (e.g., Kiefer et al. 2009), which both impact upon the rate of entrainment of ambient air into the plume and therefore its dynamics.
In Stage (ii) of this project we use idealised meteorological modelling to explore the response of bushfire plumes embedded in realistic boundary layer turbulence, to different background winds. This includes a range of constant background winds. In the final study the response of the plume to boundary-layer rolls, in the Idealised model, is examined.

As boundary-layer rolls are a central theme to both Stages of the project we include a review of boundary-layer rolls here.

1.3 Boundary-layer rolls

Boundary-layer rolls are linearly organised, quasi-two-dimensional horizontal vortices with axes approximately aligned with the mean wind that occur in the atmospheric boundary layer (Atkinson and Zhang 1996). They are secondary circulations imposed on the mean background flow and are important because:

(i) they contribute to wind speed and direction variability at the surface, which in turn influences pollution dispersion (Mahrt 2011) and the rate of spread of wildfires (Sun et al. 2009);

(ii) they are responsible for a substantial fraction of the vertical flux of momentum, heat, moisture and other scalars within and out of the atmospheric boundary layer (Brooks and Rogers 1997; Brümmer 1999; Marsham et al. 2008);

(iii) they influence the timing and location of the initiation of deeper, moist convection by modulating boundary-layer thermodynamics (Huang et al. 2009), which in turn has been observed to directly lead to severe weather such as thunderstorms (Weckworth 2000) and tornadoes (Wilson et al. 1992);

(iv) they are responsible for the generation of gravity waves in the free troposphere (Lane and Clark 2002; Worthington 2002) which leads to an influence on tropospheric circulation (Fritts and Alexander 2003);

(v) they enhance the variability of aerosol concentration and primary sea-salt aerosol production in the marine boundary layer (Kapustin et al. 2012); and

(vi) they occur in the hurricane boundary layer (Morrison et al. 2005) where they have implications for air–sea momentum exchange and intensification (Zhang et al. 2008), wave runup and potential wind damage (Ellis and Businger 2010).

Etling and Brown (1993) and Young et al. (2002) provide comprehensive reviews of the observational, theoretical and numerical studies of boundary-layer rolls and what is known about their nature. Rolls can be formed by dynamical instabilities, such as parallel instability or inflection-point instability, or by thermal instability in the weakly convective boundary layer. Both instability mechanisms can occur together, and interaction between boundary-layer convection and gravity waves in the troposphere can also influence roll dynamics. In the case of rolls caused by thermal instability, which are the most commonly observed rolls over land, the aspect ratio of the rolls (the ratio of the horizontal distance between successive updrafts to the vertical extent of the circulations) was shown by Kuettner (1973) to be 2.83 from linear theory. Various observational and numerical studies, as collated in Young et al. (2002), have since reported roll aspect ratios of that order for convectively forced rolls over land.

The presence of boundary-layer rolls becomes obvious when cumulus clouds form at the boundary-layer top, above the updraft branch of the roll circulation, resulting in linear cloud streets (e.g., Figure 1.1). The updrafts within boundary-layer rolls tend to be narrower than the downdrafts, (e.g. Glendening 1996; Liu et al. 2004), and must therefore be more intense, as dictated by continuity constraints. Because the updraft branch may be as thin as the width of one thermal, the cumuli that form at the mixed-layer top may take on a “pearls on a string” appearance, rather than being strictly linear. These cloud streets are typically aligned along, or within 10–20° of, the mean boundary-layer wind vector. In addition to the alternate updrafts and downdrafts, boundary-layer rolls also have an impact on both the speed and direction of the surface winds due to the horizontal wind components of the secondary circulation. The wind direction variability manifests itself as convergence beneath and into the updrafts and divergence below and out of the downdrafts, and the wind speed variability manifests itself as regions of reduced wind speed beneath the updrafts and elevated surface wind speed beneath the downdrafts. In addition to this spatial variability on the roll scale,

there is also a temporal variability at any given point, due to meandering and lateral propagation of the rolls.

Weckwerth et al. (1997) studied the environmental conditions conducive to the formation of boundary-layer rolls over land, using both observations and numerical modelling. A moderate surface heat flux and some vertical wind shear were found to be necessary for roll formation. The shear did not have to necessarily extend throughout the boundary layer, just be present in the near-surface layer. The mode of convection was compared to the ratio $R = -z_i / L$, where z_i is the boundary-layer depth and L is the Monin-Obukhov length, to quantify the effects of shear and surface heating on roll behaviour. Convection was linearly organised into boundary-layer rolls for values of R < 10 and unorganised from values of R > 100, with a continuum of weak organisation in between.

The diurnal cycle of boundary-layer rolls over land, from pre-roll conditions, through roll formation, evolution and dissipation, was considered by Weckwerth et al. (1999), using observations from five observational cases. The evolution of the boundary-layer rolls was found to be governed by the value of R in all cases. The increase in surface heating throughout the day led to a deepening of the boundary layer and decrease in the wind shear, resulting in an increase in the value of R. The linear organisation of boundary-layer rolls decreased with increasing R, when R exceeded about 25 the convection became either cellular or unorganised. This temporal evolution of rolls over land is mirrored by the spatial evolution of convection over the oceans in a cold-air outbreak. In this case, the mode of convection varies according to distance away from the land, as seen in the observations performed by Brümmer (1999) and the modelling of Liu et al. (2004).

Historically, numerical modelling studies of boundary-layer rolls have been limited to idealised, high-resolution, large-eddy simulations, (e.g. Tian et al. 2003; Liu et al. 2004; Fovell 2005; Huang et al.

2009), due to resolution constraints. However, the resolution of NWP is becoming increasingly fine. Convection-permitting NWP models are now routinely run operationally with horizontal grid spacings of order 1 km (e.g. Tang et al. 2013), although not yet in Australia, and in research mode with horizontal grid spacings of order 100 m (e.g. Price et al. 2011). At these resolutions, we would expect NWP models to be capable of resolving these circulations. A small amount of work has previously been done to assess the ability of NWP models to resolve coherent structures within the boundary layer. However, these have considered meandering motion in the stable boundary layer (Belušić and Güttler 2010), large-scale organised cellular convection over the ocean (Vincent et al. 2012; Andrejczuk et al. 2012) and a highly idealised simulation of daytime boundary-layer convection over land (Couvreux et al. 2012). Therefore there is a need to evaluate the skill of high-resolution NWP modelling to accurately simulate boundary-layer rolls in a realistic setup.

The boundary-layer rolls that formed on Black Saturday formed in response to thermal instability associated with solar surface heating. Boundary-layer rolls were well represented in the ACCESS high-resolution NWP simulations introduced in the next Section. Inspired by the success of the boundary-layer roll simulations in ACCESS, favourable conditions for boundary-layer roll formation were introduced to the Idealised model (Section 3), in the form of a constant surface heat flux that provided the necessary thermal instability. In the next Section the two models used in this study are introduced, including a description of the model configuration and verification. In Section 3, results from the two models are presented, and a discussion of the results with a focus on impact on the fireground is included in Section 4. The project is summarised in Section 5.

2 Numerical Weather Prediction

NWP models use relevant laws of physics to model the changing state of the atmosphere. Those laws include the equations of fluid flow, the laws of thermodynamics, the interaction between electromagnetic radiation and gasses, the physics of moisture including phase changes (e.g., evaporation and condensation), and an equation of state describing the relationship between atmospheric density, temperature, pressure and humidity. The atmosphere is approximately represented by a three-dimensional grid, and these laws are applied at each grid point to predict the state of the atmosphere a short time (typically seconds to minutes) into the future. Estimates of the future state of the atmosphere on time scales of hours to weeks (weather forecasts) are obtained by taking many such time steps.

The realistic atmosphere modelling study uses ACCESS, which has the UK Met Office Unified Model as its NWP core. The idealised modelling study uses the UK Met Office Large Eddy Model (LEM).

2.1 ACCESS

The numerical forecast process has been developed to a high level of sophistication in recent decades, with forecasts now exhibiting useful skill out to a week or more. Running such a forecast requires two types of information: an initial condition and boundary conditions. The initial condition, or analysis, is an estimate of the three-dimensional atmospheric state at the forecast start time, and is usually prepared by blending a short-term forecast from a previous analysis with all available satellite and *in situ* observations. The boundary conditions include data on topography, sea-surface temperatures, vegetation type, soil moisture, and other land and ocean surface parameters.

The number of grid points in NWP models is typically limited by computing resources. The more grid points used the better atmospheric features are resolved[1], but at the cost of increasing computation expense. Global models predict the weather for the entire atmosphere, but the large horizontal extent necessitates relatively coarse resolution. Finer resolution requires that the forecast be restricted to a limited area, and that the forecast be "nested" within a larger-scale forecast to provide an estimate of how conditions vary along the boundaries of the finer-resolution domain – this allows weather systems to migrate into (and out of) the limited-area domain. Very fine resolution can be achieved by successive nesting steps. In this project, a grid spacing of down to 0.004° (about 440 m) was used, which required four levels of nesting from the global-domain model, and effectively amounts to five separate model runs in total. Some of these model runs are discussed below, and are referred to by their horizontal grid spacing (e.g., the finest resolution model run is referred to as the 0.004° simulation). As an example, the domains for the three finest resolutions in the Black Saturday simulations are shown in Figure 2.1.High-resolution modelling of this nature provides additional information for two main reasons. Firstly, the successively higher resolution nests can use more detailed topography and other boundary conditions, to which the simulated atmosphere can then respond. Secondly, the modelled atmosphere can itself generate fine-scale structures such as very strong temperature gradients across cold fronts. The higher-resolution simulations can more accurately depict the natural processes that cause these structures, and thereby better resolve them.

[1] The smallest feature that can be represented in a model is twice the grid spacing, but the evolution of such small features is not accurately modelled. The smallest feature for which the flow dynamics are well represented is somewhat larger – for example, Skamarock (2004) suggests that this length scale is about seven times the grid spacing in the WRF model. Hence a distinction is made between the grid spacing which is specified in advance and the resolution which is an emergent quantity of the model.

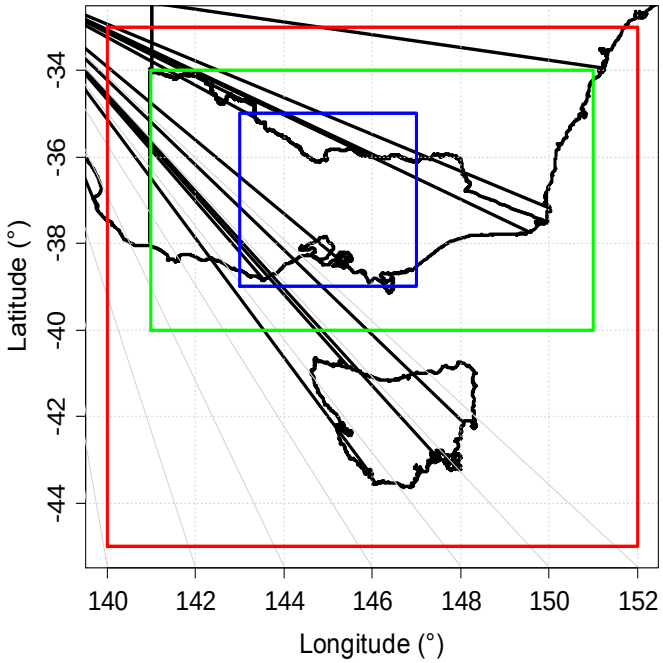

Figure 2.1: Boundaries of the third (0.036° grid spacing, red), fourth (0.012° grid spacing, green) and fifth (0.004° grid spacing, blue) nesting levels for the Black Saturday model runs. Model boundaries are chosen, as far as is possible, to avoid areas of elevated topography. The 0.036°-grid-spacing model run is nested in a large regional model (0.11° grid spacing) comprising all of Australia and surrounding areas of the oceans.

2.1.1 ACCESS Configuration

The routine operational ACCESS configuration employs sub-grid scale parameterisations for vertical mixing in the boundary-layer (Lock et al. 2000) on the lowest 13 model levels and cumulus convection (Gregory and Rowntree 1990). A number of modifications are made to this default configuration for the simulations used in this study, in order to make the model more suitable for investigating small-scale atmospheric phenomena including boundary-layer structures and the associated wind direction variability.

1. At horizontal grid spacings of less than 0.036° the convection scheme is not used because at these grid spacings the model is able to explicitly resolve convection, and the use of a parameterisation scheme for cumulus convection is no longer required.
2. At horizontal grid spacings of less than 0.012° the model starts to resolve the eddies in the boundary layer responsible for vertical mixing, making the use of a boundary-layer scheme less suitable. At these resolutions the boundary-layer scheme is turned off and the two-dimensional Smagorinsky (1963) horizontal sub-grid diffusion scheme is also applied in the vertical, employing a fully three-dimensional sub-grid diffusion scheme.

2.1.2 ACCESS Verification

Weather forecasts continue to improve, but are never perfect. One source of error arises because the model itself is not exact: a finite grid spacing is used and some important physical processes, such as turbulence and convection, have to be approximated. Another source is inexact initial and boundary conditions. A third source is the chaotic nature of the atmosphere, in which small initial errors or uncertainties grow exponentially and eventually swamp useful information in the forecast. It follows that verification of NWP forecasts and hindcasts is very important.

For this part of the project, two main verification approaches were used: (i) direct verification of wind, temperature and moisture from observing sites, and (ii) object-oriented verification in which the location and/or timing of suitable meteorological features is verified. An example of object-oriented verification is the timing of the wind change on Black Saturday. Figure 2.2 shows the difference in timing of the wind change between the model and automatic weather stations (AWSs). Figure 2.3 compares the location of the wind change at four-hour intervals from the 0.036° and 0.012° simulations, to that analysed by the Bureau of Meteorology (BoM 2009b, VBRC 2010, expert estimates of the wind-change position based on all available observations). The other technique was

direct verification against observations. The simulated data were compared to all available AWS observations within the model domain, enabling a qualitative assessment to be made of the model accuracy. An example of this type of verification can be seen in Figure 2.4, which shows the observed one-minute-interval data at Eildon Fire Tower (the closest AWS to the Murrindindi fire), together with the modelled five-minute-interval data at the nearest grid point. Full verification of the simulations, together with detailed discussion, can be found in various project reports and other publications, including Fawcett et al. (2012a,b, 2013a,b,c,d,e,f,g), Kepert and Fawcett (2013a,b), and Kepert et al. (2012a,b, 2013).

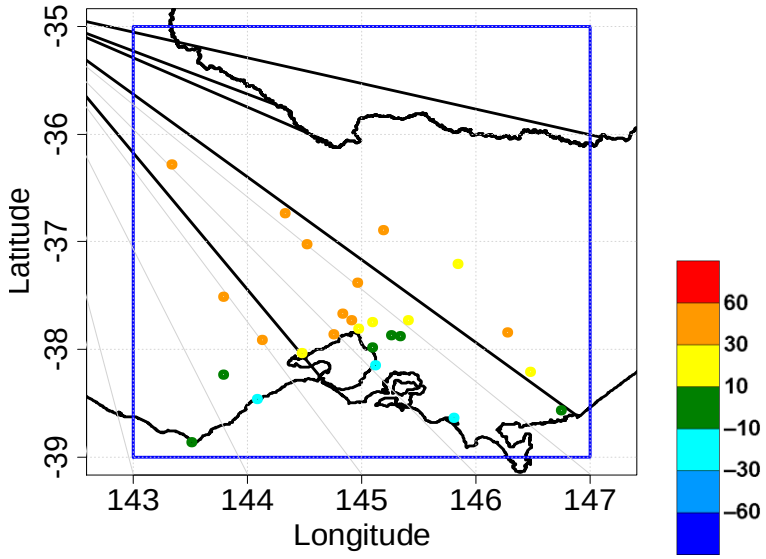

Figure 2.2: Approximate timing errors in minutes for the location of the primary wind change on Black Saturday. Positive (negative) values imply that the primary wind change in the 0.004° simulation is late (early) relative to the change at the indicated AWS locations. The blue box denotes the model domain boundary.

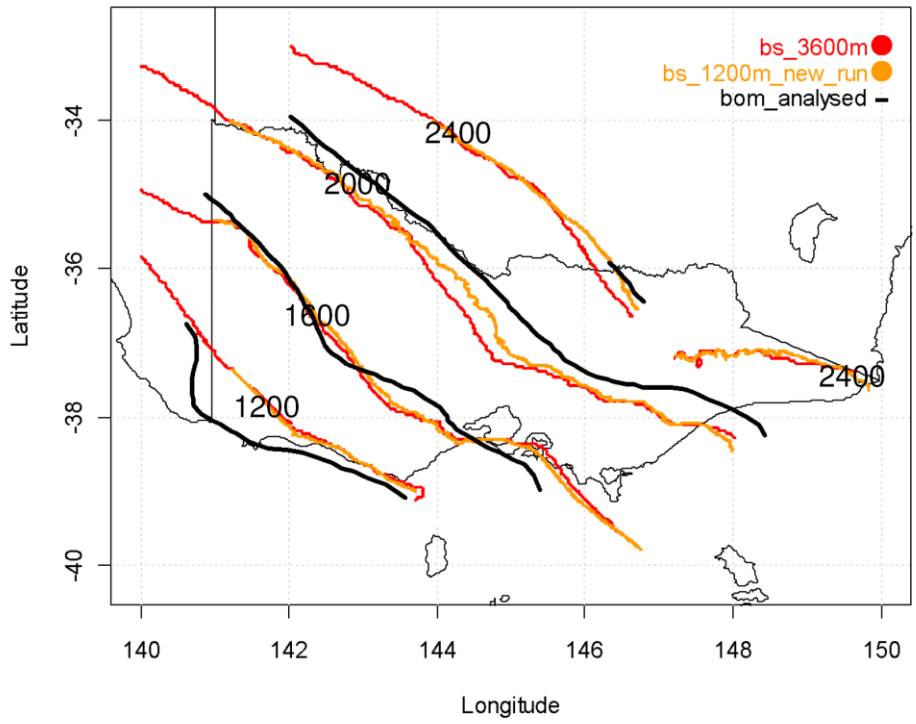

Figure 2.3: Comparison of analysed primary wind-change positions (black lines) with model wind-change positions from the 0.036°- grid spacing (red lines) and 0.012°- grid spacing (orange lines) simulations, for 1200, 1600, 2000 and 2400 EDT on Black Saturday. Analysed wind-change positions are from BoM (2009b) and VBRC (2010). Modelled wind-change positions are determined semi-objectively from the 10-metre wind direction field.

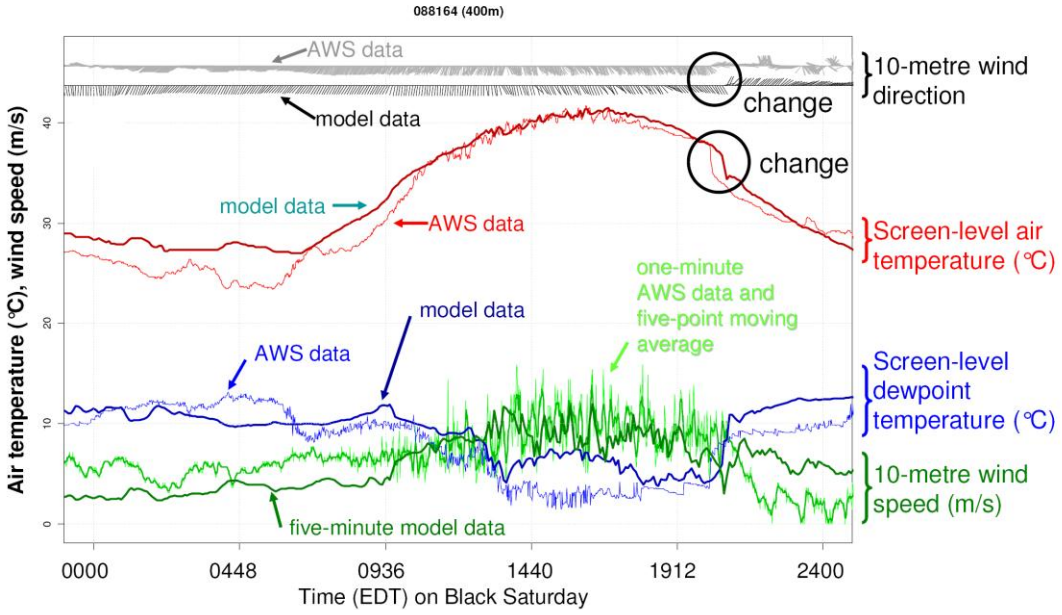

Figure 2.4: Wind, temperature and moisture time-series from the 0.004°- grid spacing Black Saturday simulation (thick lines) against one-minute interval observations from the Eildon Fire Tower (thin lines). Meteorological variables are as annotated on the diagram. The timing of the change is highlighted by the circles in the wind direction and temperature data. Wind direction lines indicate the direction the wind is travelling towards.

2.2 Large-Eddy Model

In the original project plan, high-resolution ACCESS simulations for investigating the updraft phenomena of interest were proposed. However, further investigation into both the fire weather literature and the ACCESS modelling system revealed that ACCESS would not be suitable for the task. A careful review of other modelling options was undertaken, which identified the UK Met Office Large-Eddy model (LEM, Gray et al. 2001) as the best tool for the task. The LEM is quite similar to ACCESS in many ways. The same laws of physics are represented, and very similar methods are used to integrate the atmospheric state forward in time. The main difference is the ability to create Idealised initial and boundary conditions, and the ability to turn on and off various physical processes. It can also be run at much higher resolution than ACCESS. Very high resolution enables plume entrainment and detrainment to be resolved, which is very important for reproducing realistic plume behaviour. The main advantage of idealised modelling is that experiments can be more easily controlled, which makes it considerably easier to identify cause and effect.

As this is the first time the LEM has been used by our research team, it is worth documenting in detail relevant background information, making comparisons with ACCESS and demonstrating its suitability for studying fire–atmosphere interactions. The LEM is an idealised, three-dimensional high-resolution non-hydrostatic atmospheric model which solves a quasi-Boussinesq (anelastic) equation set on a three-dimensional Cartesian grid. The sub-grid stresses are parameterised using a stability-dependent version of the Smagorinsky-Lilly scheme, described by Brown et al. (1994). It has been used to successfully simulate a wide range of atmospheric problems, including dry turbulence, tracer transport, dry and moist boundary layers, and shallow and deep moist convection. The simulations presented here are performed using Version 2.4 of the LEM.

Recently the LEM has been used to simulate the plume produced by the Buncefield fire (Devenish and Edwards, 2009), the largest fire in Europe since the Second World War (Figure 2.5).

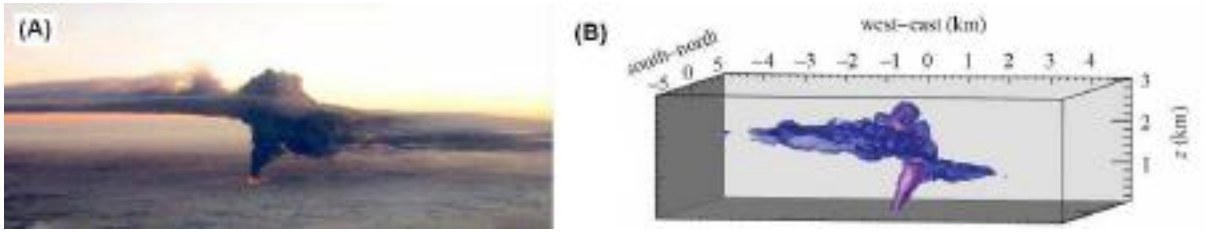

Figure 2.5: (A) Observed Buncefield fire plume and (B) LEM modelled Buncefield fire plume, after Devenish and Edwards (2009).

The main difference between NWP models such as ACCESS and the LEM is the grid spacing. LEMs typically operate on grids with horizontal spacings of the order of tens of metres, in contrast to NWP models that even at their highest resolution operate on grids with horizontal spacing of the order of hundreds of metres to kilometres. The smaller grid spacing of an LEM allows it to explicitly resolve more physical processes and therefore fewer processes need to be parameterised. Most importantly, in our case, LEMs explicitly resolve large eddies in the atmosphere. This means they are of a high-enough resolution to be capable of not only resolving the plume itself, but also of resolving the turbulent eddies responsible for mixing air into and out of the plume, which determines the change in plume buoyancy and hence plume updraft strength and final height.

Recent advances made with the ACCESS model have allowed it to be run with horizontal grid spacings of the order of hundreds of metres, effectively as a coarse LEM: however it is currently unsuitable for fire plume studies. The main problem results from a technical restraint of having an integer timestep in the version of the ACCESS model available to us that limits the minimum timestep to 1 s, which in turn puts a lower bound on the horizontal grid spacing that is too large for fire plume studies. The idealised nature of the LEM also makes it comparatively easy to set up simulations with a range of background winds, and fires represented by surface heat-flux anomalies.

In contrast, it would be quite a technical challenge to achieve this with a “real-world” operational forecast model such as ACCESS. By default the LEM also outputs a larger ranger of model diagnostic variables than ACCESS, primarily relating to the turbulent properties of the atmosphere. These are important for evaluating mixing processes that strongly influence the strength of the plume.

2.2.1 LEM - Model Configuration

A standard set of simulations was performed on a domain with horizontal dimensions of 768 by 384 grid points, with a uniform grid spacing of 50 m in both directions, resulting in a domain size of 38.4 km by 19.2 km (Figure 2.6). This domain has 256 grid points in the vertical, made from a stretched grid specified with a vertical grid spacing of 10 m near the surface, increasing smoothly to 50 m above a height of 3 km and leading to a model top at 10 km. The lateral boundary conditions of the model are doubly periodic and a no-slip condition is applied at the lower boundary, with a specified roughness length of 0.05 m. The domain size chosen is large enough for the periodic lateral boundary conditions not to affect the simulated plumes to any significant extent. At the model’s upper boundary, a free-slip condition is applied in conjunction with a Newtonian damping layer in the top 2 km of the domain, to prevent the reflection of vertically propagating gravity waves. Our simulations are performed without any radiation, moisture or microphysics and the Coriolis force is also ignored.

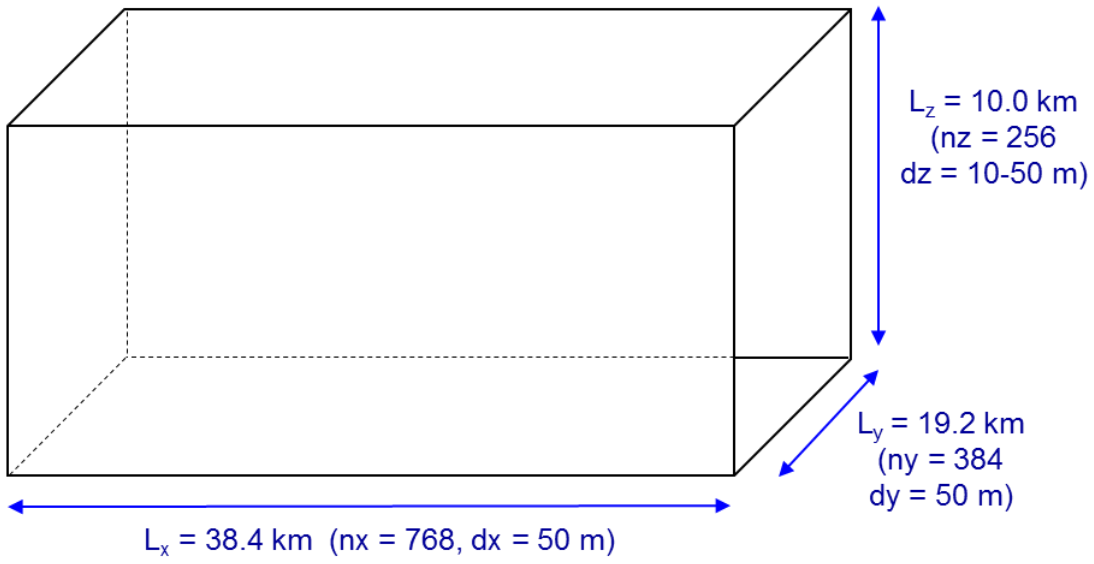

Figure 2.6: LEM domain dimensions and grid spacing.

Before modelling the plume itself, a realistic atmosphere is set up. As is customary with large-eddy modelling, we initialise the model with horizontally homogeneous initial conditions, presented in Figure 2.7. These are designed to be representative of conditions that may be typical on a high fire-danger day. The potential temperature is constant from the surface to a height of 3 km, from where it increases linearly at a rate of 3 K km^{-1} to the model top. The velocity in the x-direction, *u*, is set to a value that is constant with height (u_{TOP}) and *v* is set to zero. To introduce turbulence into the model, random potential temperature perturbations of amplitude ±0.2 K are added to the potential temperature below 3 km before the simulation commences.

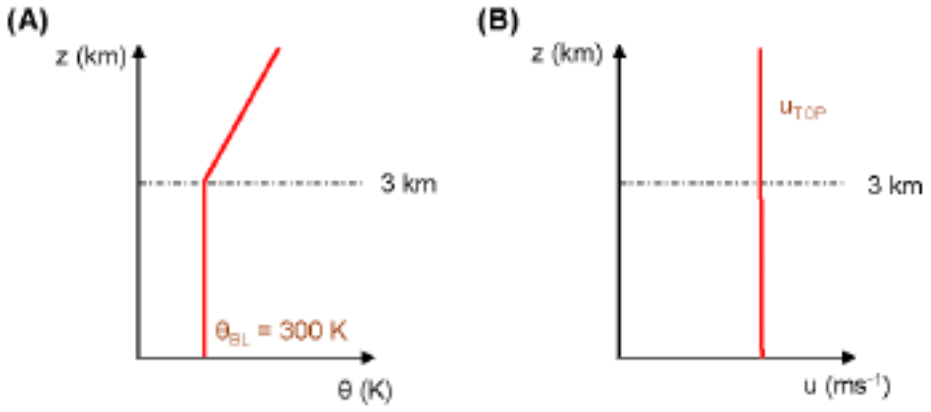

Figure 2.7: LEM initial conditions; (A) potential temperature, K, and (B) velocity, m s^{-1}.

To ensure a realistic atmosphere at ignition time, the model is run for a few hours (dependent on the value of u_{TOP}) to allow turbulent processes to develop. This step, which was not included in a number of earlier studies (e.g., Kiefer et al. 2009), allows realistic temperature and velocity profiles to develop. These realistic profiles are important to accurately represent large-scale plume advection, and the development of realistic eddies that ensure the mixing of air into and out of the plume is accurately modelled. The fire is represented by imposing a circular surface heat flux anomaly into the model domain, similar to Devenish and Edwards (2009). A passive tracer is emitted from the fire area at a constant rate, to aid visualisation of the plume.

In the second phase of the LEM experiments (the study of plume interaction with boundary-layer rolls), a surface heat flux of 50 W m^{-2} was applied across the entire domain during both the spin-up and plume phases to provide the thermal instability necessary for boundary-layer roll development. Some experimentation to identify the best domain geometry was performed, with the best result being the same as for the previous experiments. Thus the only change to the system for the boundary-layer roll study was the introduction of the surface heat flux.

2.2.2 LEM - Model Validation

As the LEM simulations are idealised, the experiments cannot be verified directly. However, the realistic wind and temperature profiles, and turbulent characteristics that develop after the few hours of spin-up, mentioned above, can be assessed, thereby providing a degree of model validation. Such profiles and turbulent characteristics have been well observed and studied for cases with and without surface heating. Here we first show examples for the case without surface heating with u_{TOP} = 15 m s^{-1}, before showing results from the same setup but with the constant 50 W m^{-2} surface heatflux.

Wind and temperature profiles after 10 hours of model spin-up for an example in which u_{TOP} = 15 m s^{-1} and is shown in the upper panel of Figure 2.8. The average potential temperature profile (Figure 2.8a upper) has only been modified slightly from the specified initial conditions, with a small smoothing of the transition point at the top of the mixed layer where the constant potential temperature zone meets the constant potential-temperature gradient zone. The modification of the average velocity profile (Figure 2.8b upper) is much more marked. The velocity at the surface has reduced to zero and a log layer[2] has developed above it, as highlighted by the profile replotted on a log-height *y*-axis (Figure 2.8c upper). In fact, the velocity at the surface reduces to zero very early on in the simulation, but the log layer only develops once the resolved mixed-layer turbulence has spun up (not shown).

Wind and temperature profiles after three hours of model spin-up for the surface heating example with u_{TOP} = 15 m s^{-1} are shown in the lower panels of Figure 2.8. The addition of surface heating leads to small but notable differences in the potential temperature and zonal wind profiles. A surface super-adiabatic layer is evident, with a deeper and slightly warmer boundary layer. With respect to the zonal wind the log layer is much shallower (about 100 m compared with 1000 m in the non-heating case), and the wind speed is nearly constant above the log layer throughout most of the boundary layer, which is suggestive of very efficient mixing.

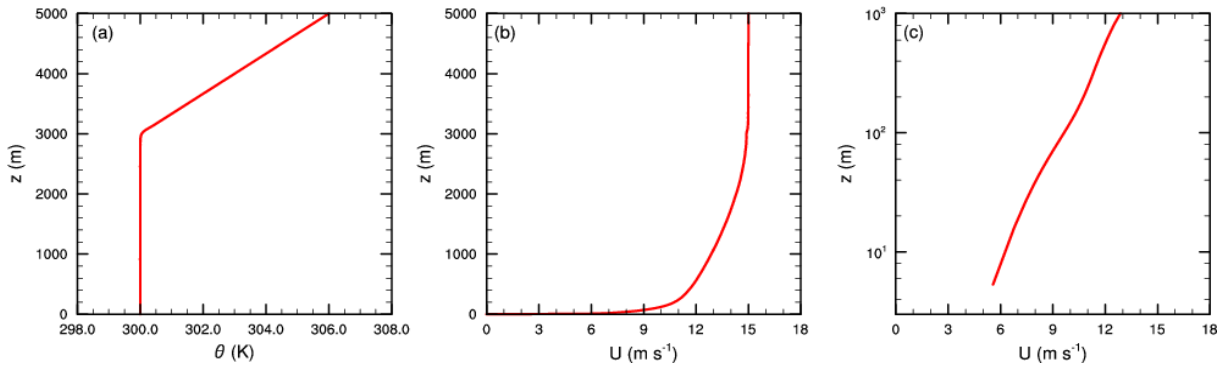

[2] The log layer refers to wind speed that varies logarithmically with height above the surface.

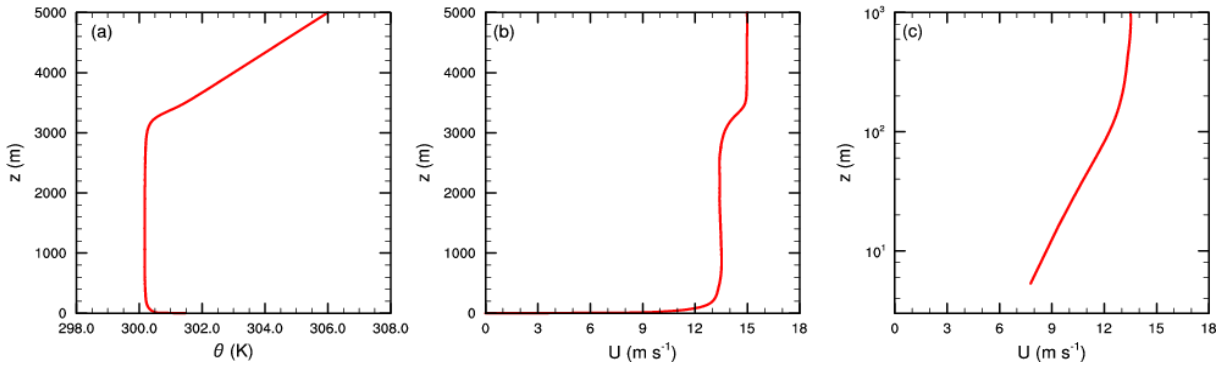

Figure 2.8: Domain-averaged profiles of the mean condition in the 15 m s^{-1} background-wind simulation at quasi-steady state for the zero surface heating case (upper panel) and the 50 W m^{-2} heating case (lower panel, used in the boundary-layer roll experiments). (a) Potential temperature, K; (b) velocity, m s^{-1}; and (c) velocity, m s^{-1}, plotted on a logarithmic height scale.

Figure 2.9 shows the time series of the domain-averaged turbulent kinetic energy (TKE) in the 15 m s^{-1} simulation from the no-surface-heating case. After about 550 minutes of model time the resolved mixed-layer turbulence has fully spun up and the model has reached a quasi-steady state. The form of the timeseries plots is similar for each value of u_{TOP}, although the simulations with higher values of u_{top} reach quasi-steady state earlier in time than the simulations with lower values of u_{TOP}. The exception to this is the u_{top} = 2.0 m s^{-1} case (the weakest wind case simulated), in which the resolved mixed-layer turbulence does not spin up at all over the period simulated. Interestingly, the quasi-steady state TKE developed in almost half the time (3 hours) in the case with surface heating (not shown). However, unlike Figure 2.9 the TKE continued to grow slowly with time due to the continued energy source from the surface heating.

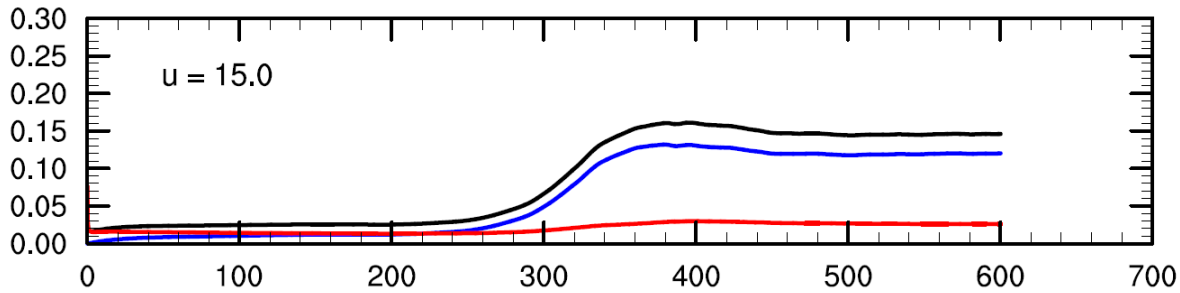

Figure 2.9: Timeseries of the domain-averaged vertically integrated turbulent kinetic energy (TKE, units $J\ m^{-2}$) in the 15 m s^{-1} background wind simulation. The resolved TKE is plotted in blue, the sub-grid TKE is plotted in red and the total TKE is plotted in black.

The domain-averaged profiles of the velocity variances, $\overline{u'u'}$ and $\overline{w'w'}$ and the vertical flux of horizontal momentum, $\overline{u'w'}$, are presented in the upper panels of Figure 2.10. The profiles of these quantities and their partitioning into resolved and sub-grid components are in good agreement with previous studies of the neutral, shear-driven boundary layer (e.g., Mason and Thomson 1987; Andren et al. 1994; Moeng and Sullivan 1994) indicating that we have generated a realistic neutral atmospheric boundary layer. Equivalent plots for the surface heating case are presented in the lower panel of Figure 2.10. The profiles of these quantities and their partitioning into resolved and sub-grid components are also in good agreement with previous studies of the neutral, convective boundary layer (e.g., Moeng and Sullivan 1994) indicating that we have generated a realistic dry-convective atmospheric boundary layer.

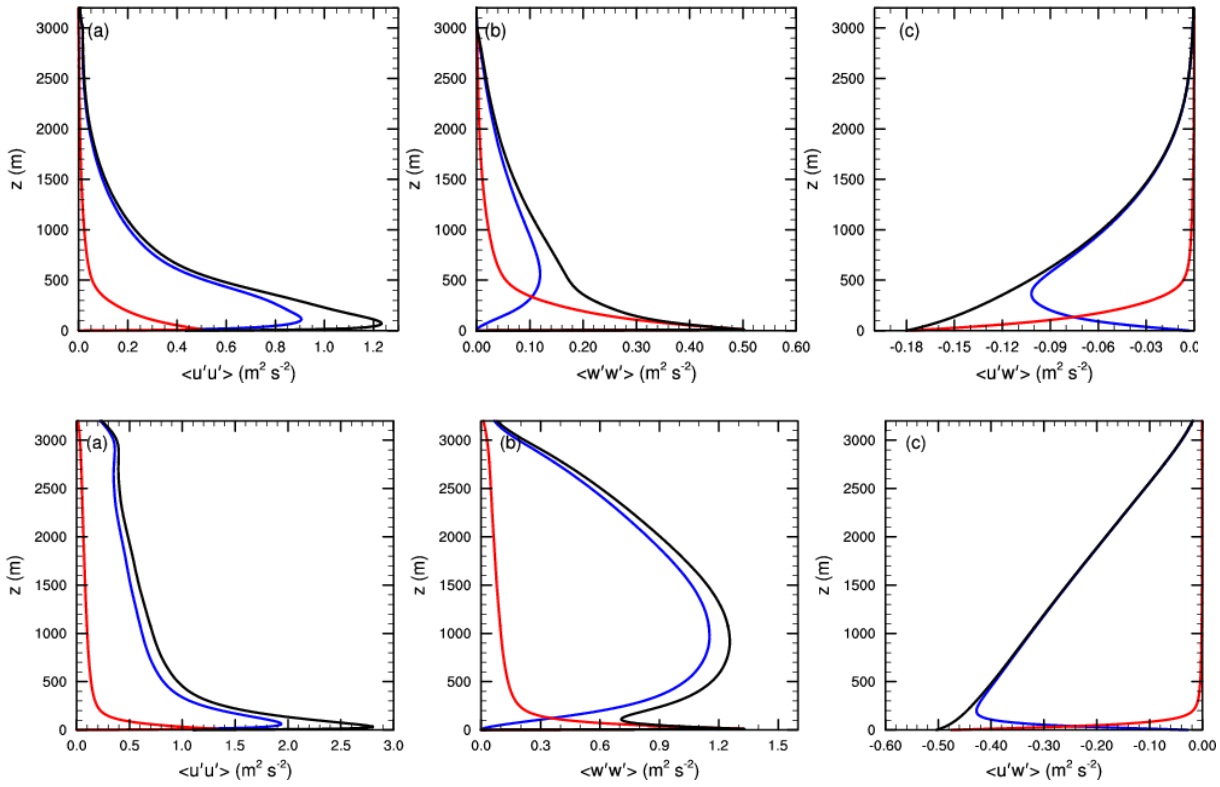

Figure 2.10: Domain-averaged profiles of the velocity variances and vertical momentum flux in the 15 m s^{-1} background-wind simulation at quasi-steady state for the zero surface heating case (upper panel) and the 50 W m^{-2} heating case (lower panel, used in the boundary-layer roll experiments). (a) $\overline{u'u'}$, $m^2 s^{-2}$; (b) $\overline{w'w'}$, $m^2 s^{-2}$; and (c) $\overline{u'w'}$, $m^2 s^{-2}$. In each panel the resolved component is plotted in blue, the sub-grid component in red and the total in black. The negative values in (c) represent a downward momentum flux.

3 Modelling results

3.1 Boundary-layer Rolls Study – ACCESS

3.1.1 The Meteorology of the Black Saturday Fires.

Black Saturday, 7 February 2009, was the worst fire disaster in Australia's recorded history, with 173 deaths, thousands of houses and other buildings destroyed, and major environmental damage (VBRC 2010). The fires followed a decade-long drought (1997 to2008; BoM 2008, Timbal 2009, Timbal and Fawcett 2013), and a severe heatwave (BoM 2009a) in the preceding week, which combined to cause extremely dry fuels. The fires spread exceptionally quickly, both directly and due to spotting over distances exceeding 30 km (Cruz et al. 2012), and were extremely intense. The weather on the day itself was broadly similar to earlier major disasters in southeast Australia such as Black Friday in 1939 and Ash Wednesday in 1983, with hot dry gusty northerly winds preceding a strong south-westerly change. As in the earlier events, the majority of the deaths occurred close to the change.

The quality of the simulations presented here was high. Screen-level maximum temperatures were very accurately predicted, humidity somewhat less so, while the 10-metre wind speeds showed a consistent negative bias typical of NWP systems. The timing of the change was within an hour of that observed or analysed, which was substantially better than the previous operational limited-area modelling system (Limited Area Prediction System, LAPS) used in the Bureau, which was operational at the time. A small ensemble of ACCESS runs was made by running the model from initial conditions from two NWP centres and four different initialisation times. The spread of timing of the primary wind-change from this ensemble is consistent with the actual timing error.

The simulations showed a wealth of fine-scale detail, including the complex time-varying structure of the wind changes, the development of boundary-layer rolls and their transition to cellular convection, and the development of fine-scale vortices on the wind changes. Of particular interest to this study is the wind variability and enhanced lofting potential of the boundary-layer rolls, discussed further below. The ability of the model to reproduce such features is very encouraging. Verification of such features showed that the model very often generated them in about the correct time and place. Before describing the boundary-layer rolls in detail, we provide a brief overview of the other small-scale features.

The main wind change originated from a synoptic-scale trough reinforced by a land-sea temperature contrast along the Victorian coast to the west of Cape Otway, which began to propagate to the north-east around dawn. There was a weaker, east-west oriented change over western Victoria, and several less extensive lines that originated at other coastal boundaries. This structure is apparent in the plot of surface wind and temperature at 06 UTC (1700 EDT = UTC + 11 hours) shown in Figure 3.1. The main change moved a little slower than observed during the day, but sped up during the evening such that the timing error in northern Victoria was only 15 minutes. During the afternoon, the passage of the change in coastal regions had the character of a density current, as the land sea-temperature gradient detached from the coastline and moved inland, which transitioned to a bore at night propagating on the nocturnal inversion (Figure 3.2). Radar data from Yarrawonga clearly showed the bore passage. There is strong evidence that the bore passage caused a significant intensification of the Beechworth-Mudgegonga fire plume around midnight. The modelled change had an updraft in excess of 5 m s^{-1} at 500 metres above the surface for much of the time, whether as a density current or as a bore, which is similar to the fall speed of embers and would have helped suspend and transport embers already lofted to that level by the fire plume. It is likely that it

contributed to the major outbreak of spotting at the Beechworth-Mudgegonga fire discussed in the 2009 Victorian Bushfires Royal Commission report (VBRC 2010).

The simulated change also featured a string of small-scale vortices along its length, associated with small patches of stronger winds and perturbations to the quasi-linear nature of the change (Figure 3.3). While there is no observational evidence of the existence of these features, because they are too small to be identified in the observational data, they clearly warrant further investigation given their potential impact on fire behaviour.

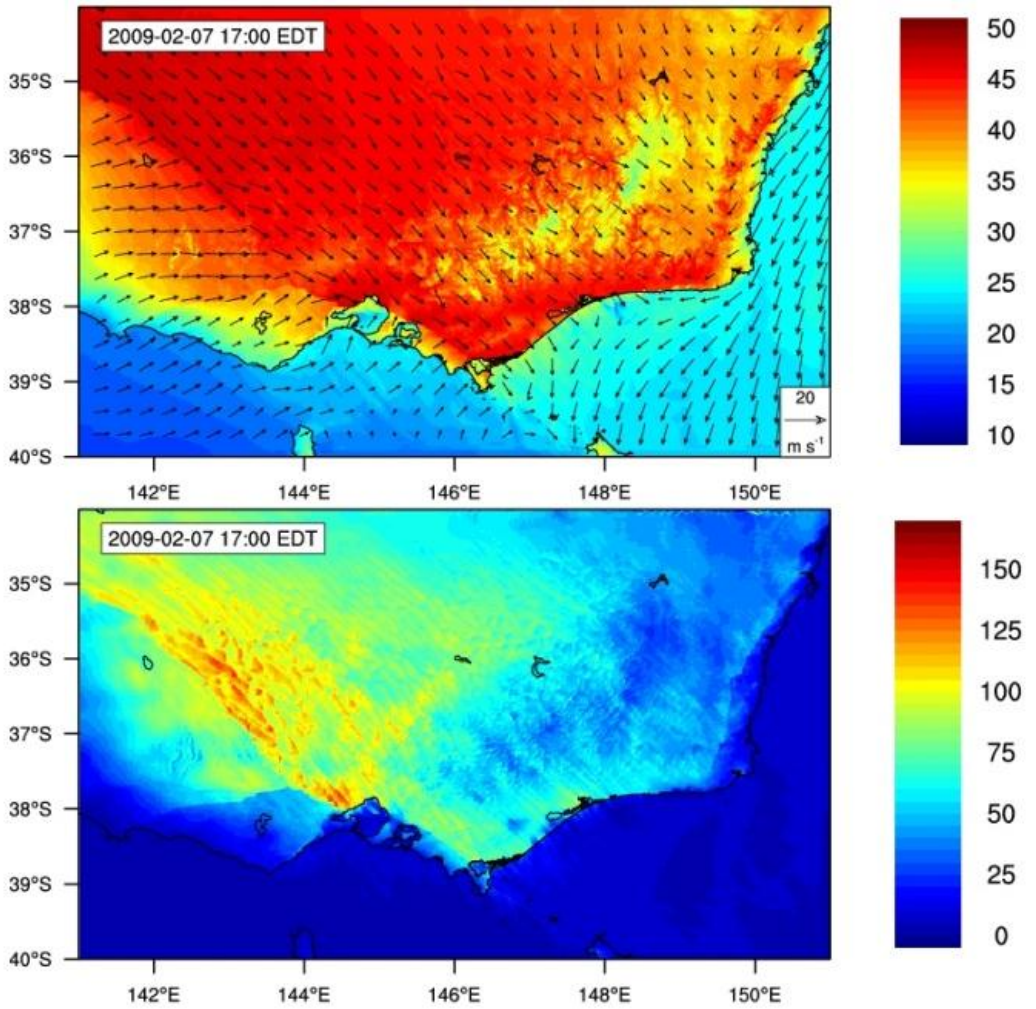

Figure 3.1: Simulation of the surface meteorology over Victoria at 1700 EDT on 7 February 2009. Top: 2-metre air temperature (colour) and wind (vectors). Bottom: Notional instantaneous Forest-Fire Danger Index (FFDI). The dual structure of the wind change to the west is clearly apparent. The variations in wind direction ahead of the change, and the fine-scale structure in the FFDI field, are due to mesoscale convective features in the boundary layer following the breakdown of the rolls.

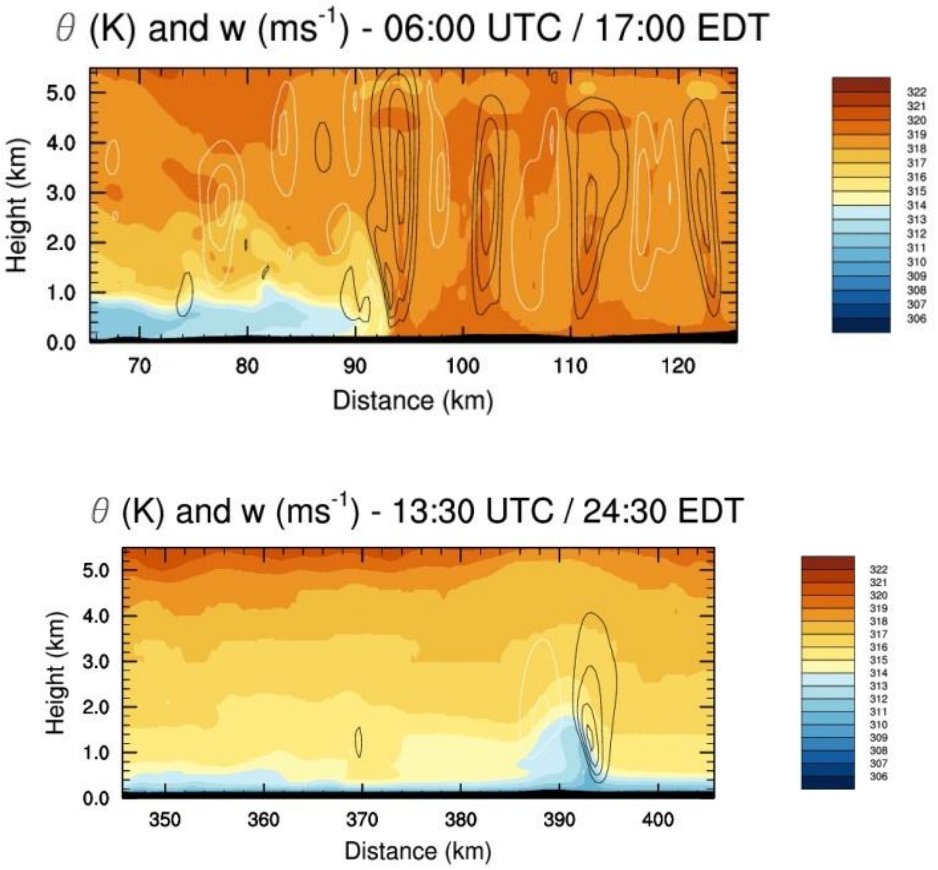

Figure 3.2: Cross-sections of potential temperature (colour, in K) and vertical velocity (contours, interval 1.5 m s^{-1}, black is upwards and white downward motion) through the wind change at 1700 EDT on 7 February 2009 (top) and 0030 EDT on 8 February 2009 (bottom). During the afternoon, the wind change has the structure of a density current propagating into the unstable boundary layer. By midnight, the change has transformed into a bore, propagating on the near-surface nocturnal stable layer.

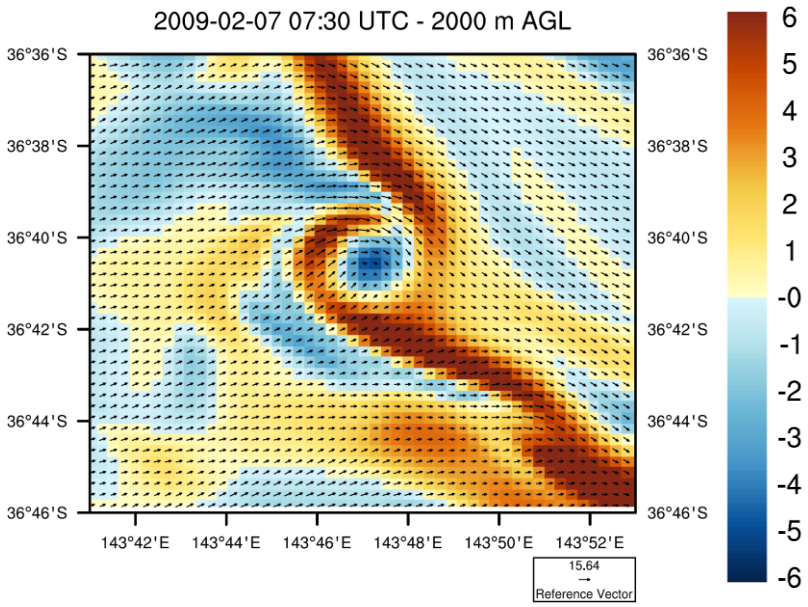

Figure 3.3: Vertical velocity at 2000 m above ground level (shading, m s^{-1}) and horizontal wind at 10 m above ground level (vectors) in one of the vortices along the wind change at 0730 UTC (1830 EDT) on Black Saturday. The wind change is represented in the model, amongst other things, by a line of updrafts (brown shades), but the centre of the vortex is modelled as having a downdraft.

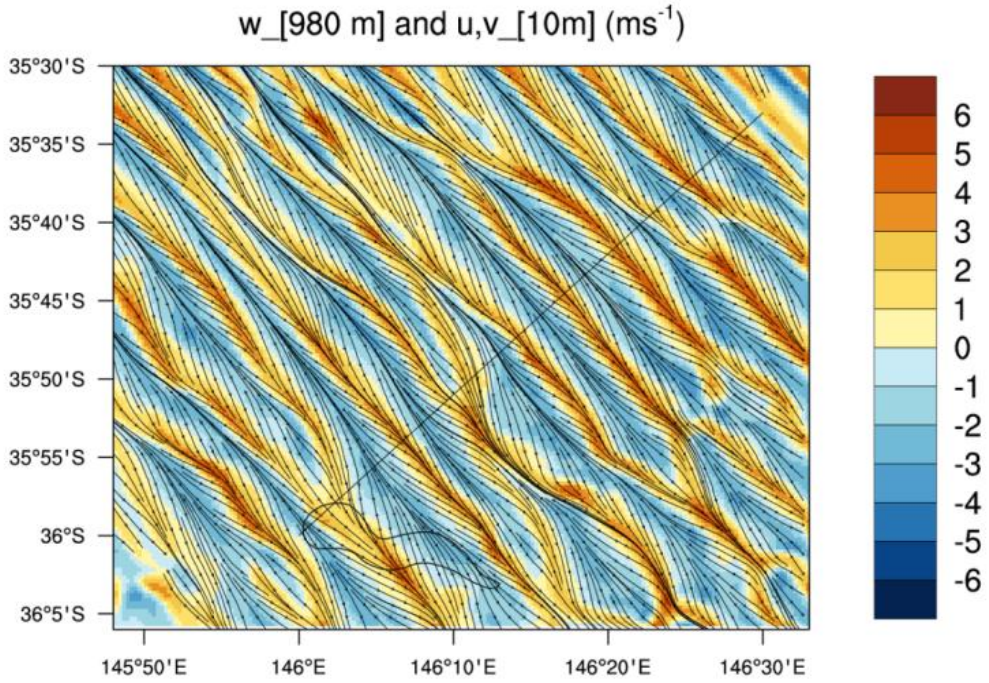

Figure 3.4: Boundary-layer rolls at 0230 UTC (1330 EDT) on the afternoon of Black Saturday. 10-m wind (streamlines) and vertical velocity (m s^{-1}) at 980 m (shading). The shoreline of Lake Mulwala is shown near the bottom of the plot.

Boundary-layer rolls

From late morning, the flow ahead of the change developed an extensive area of boundary-layer rolls. Temperatures in excess of 46 °C and north-westerly winds in excess of 70 km h^{-1} were recorded during the afternoon of Black Saturday, indicating the strongly heated and sheared nature of the boundary layer. Visible satellite imagery (Figure 3.5) illustrates the development of the cloud-topped boundary layer throughout the afternoon (see also Figure 1.1). Cumulus clouds began to form between 1230 and 1330 EDT (Australian Eastern Daylight Time, UTC + 11 h) and by 1530 EDT most of Victoria and southern New South Wales was covered by shallow cumulus convection. Interaction between the strong surface heating and high wind speeds organised the individual cumulus clouds quasi-linearly, like pearls on a string, oriented approximately north-west to south-east.

Organisation of the shallow convection is also evident in the reflectivity from the Yarrawonga radar, located at 36° 02’ S, 146° 02’ E. At 1242 EDT there is a region located to the north west of the radar in which the signal is organised into alternating bands of high and low reflectivity. The bands are oriented approximately north west to south east and have a spacing of about 7 km between successive maxima. These bands of increased reflectivity are caused by horizontal convergence in the near-surface winds, which draws clear air radar scatterers such as insects into the updrafts. (The insects being largely comprised of water and of similar size to rain drops reflect the radar beam in a similar manner to rain drops.) The region of banding persists and by 1322 EDT the spacing between bands increases to approximately 8 km. At 1402 EDT the banding covers a larger area and the spacing is about 9 km. By 1442 EDT the radar reflectivity signal has reduced, making it difficult to accurately assess the characteristic size and extent of the banding, but it appears that the organisation of the convection is becoming less linear and more cellular.

The signatures of the organised convection are also present in the surface observations, as seen at the Yarrawonga AWS (automatic weather station) collocated with the radar, Figure 3.7. The screen temperature increases throughout the morning and into the afternoon under strong surface heating and the maximum temperature of 46.0 °C is reached at 1411 EDT. There is considerable variability in the screen temperature during the afternoon, when fluctuations in temperature of up to 2 °C are observed over 10-minute periods. Similarly, as the wind speed increases throughout the morning and into the afternoon so does the variability, with fluctuations in the 1-minute-averaged 10-m wind speed as large as 10 km h^{-1} observed over just three minutes. Over the same time period the wind direction can vary by up to 40° and this direction variability increases to 60° over a 10-minute period.

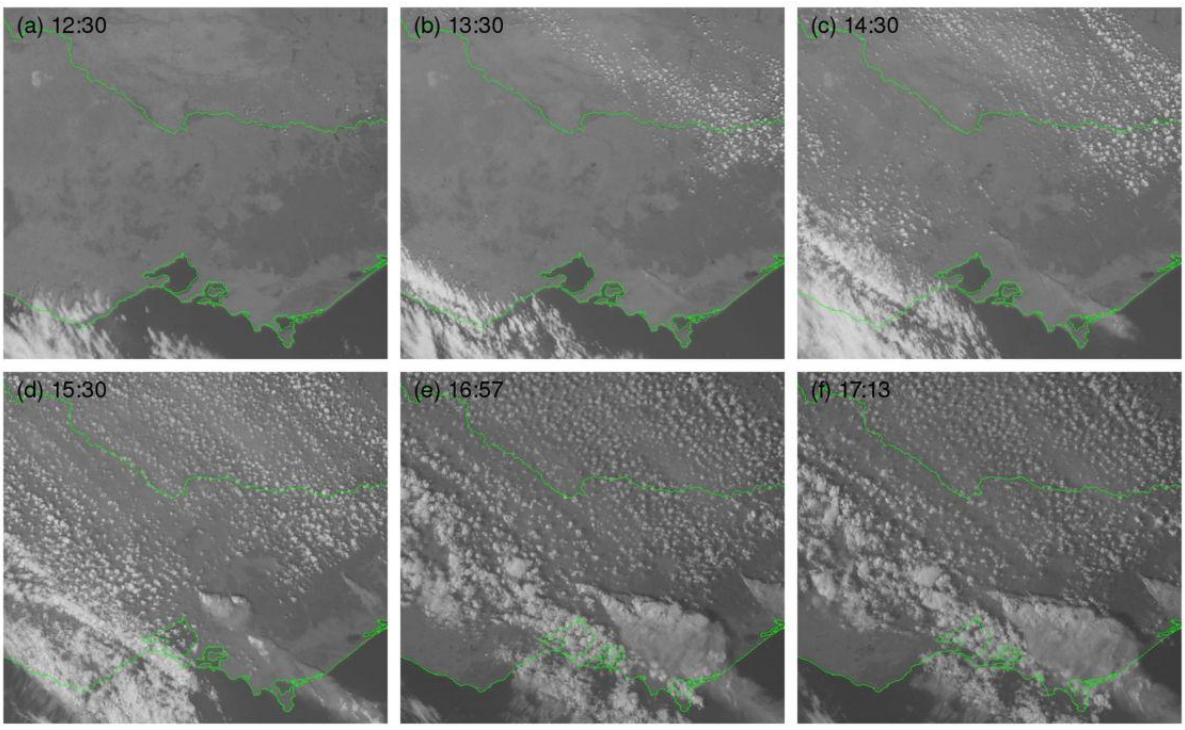

Figure 3.5: MTSAT-1R visible imagery of Victoria and southern New South Wales at (a) 1230 EDT, (b) 1330 EDT, (c) 1430 EDT, (d) 1530 EDT, (e) 1657 EDT and (f) 1713 EDT on 7 February 2009.

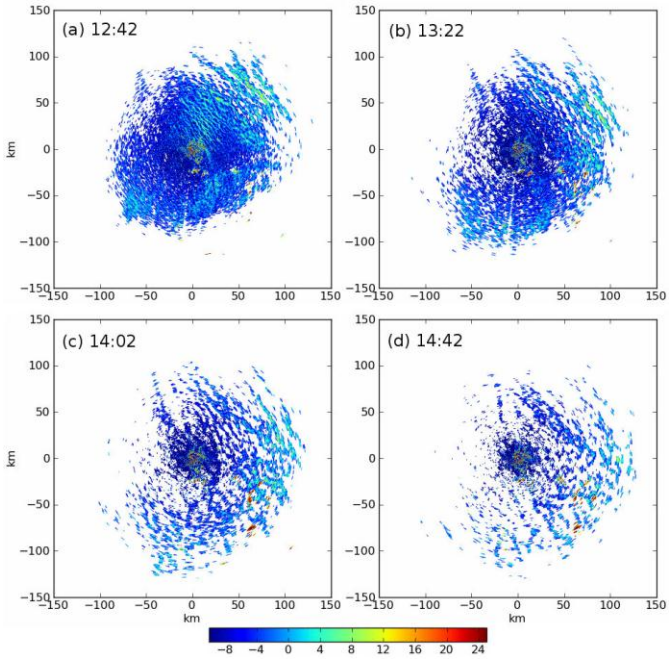

Figure 3.6: 0.9° elevation plan position indicator images of the Yarrawonga radar reflectivity (in dBZ) at (a) 1242 EDT, (b) 1322 EDT, (c) 1402 EDT and 1442 EDT, on 7 February 2009.

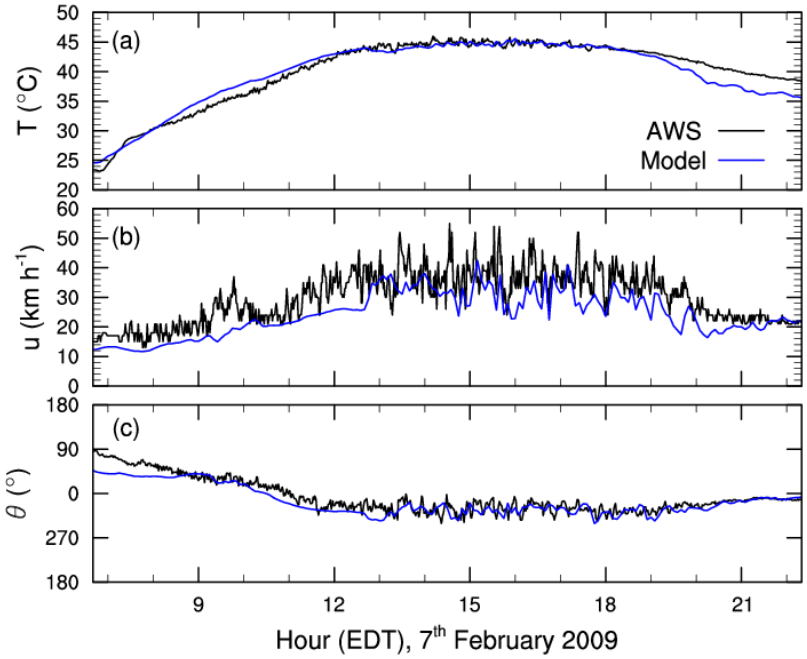

Figure 3.7: Observations and model data of (a) screen temperature (°C), (b) wind speed (km h^{-1}) and (c) wind direction (in °) at the Yarrawonga AWS (Bureau station number 081124), on 7 February 2009.

3.1.2 High-resolution ACCESS Modelling Results

The area of study chosen to investigate the wind direction variability is a small subset of the full 0.004° simulation domain. It is in relatively flat terrain that encompasses the Yarrawonga radar and AWS (to enable direct comparison with observations), and it is sufficiently far from upstream boundaries such that the air entering the domain has sufficient time for the rolls to develop.

Figure 3.8 shows cross-sections of potential temperature overlaid on vertical velocity and plan views of 10-m wind streamlines overlaid on 980-m vertical velocity, illustrating the afternoon evolution of the boundary-layer convection in our chosen sub-region. At 1245 EDT, there is a thin, near-surface super-adiabatic layer below a well-mixed layer of approximately 3 km depth. Structure to the mixed-layer convection has begun to develop, in the form of alternating updrafts and downdrafts visible in the cross-section. The updrafts are warmer and narrower than the downdrafts and are also more vigorous; the maximum updraft is in excess of 5 m s^{-1}, whereas the maximum downdraft is only about 3 m s^{-1}. Maximum updrafts occur at a height of about 1.5 km, approximately one half the mixed-layer depth, and the mean spacing between successive updrafts is approximately 5 km. The plan view shows that the updrafts and downdrafts are aligned linearly, forming boundary-layer rolls, with the surface winds converging into the updrafts and diverging out of the downdrafts.

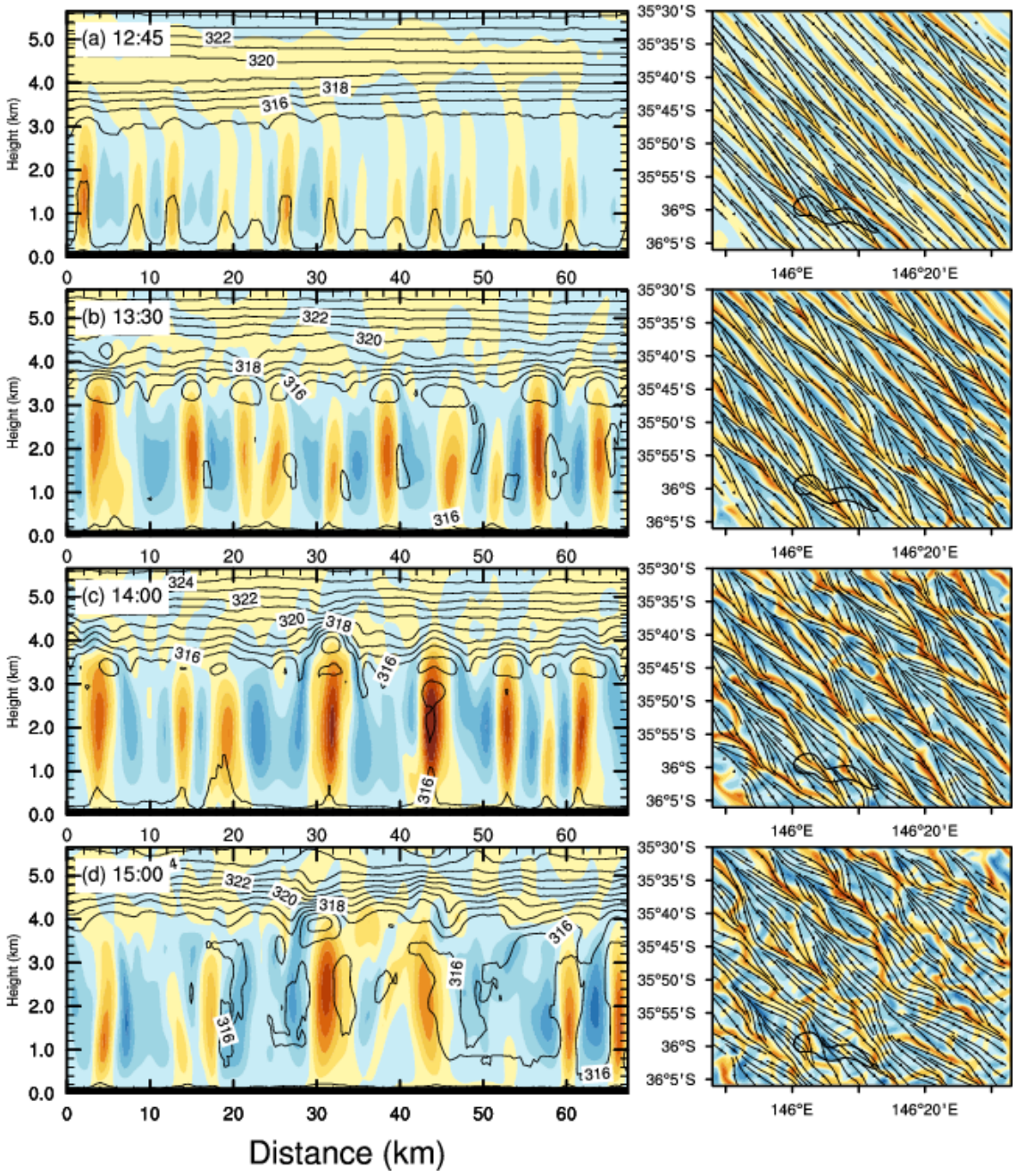

Figure 3.8: Model output from the 400 m domain at (a) 1245, (b) 1330, (c) 1400 and (d) 1500 EDT, on 7 February 2009. Left-hand panels: Vertical cross-sections of potential temperature (line contours at 1 K intervals) overlaid on vertical velocity (filled contours at 1 m s^{-1} intervals, yellow and brown shades positive, blue shades negative). Right-hand panels: Plan view of wind streamlines at 10 m above ground level overlaid on vertical velocity at 980 m AGL (filled contours at 1 m s^{-1} intervals).

By 1330 EDT, the shallow convection has intensified under strong surface heating. As a result the peak updraft increases to 6 m s^{-1} and the mixed layer deepens to about 3.4 km. The spacing between the boundary-layer rolls correspondingly increases to about 7 km and the height of the

peak updrafts is raised to just under 2 km. The linear organisation of alternating updrafts and downdrafts characteristic of boundary-layer rolls is still evident in the plan view and the variation in the surface wind direction due to the inflow and outflow has increased with the strength of convection. By 1400 EDT this intensification, deepening and broadening of the boundary-layer rolls leads to updraft speeds in excess of 7 m s^{-1}, spaced approximately 9 km apart, with a peak updraft height of about 2.0 km. In the plan view the linear nature of the boundary-layer rolls is not as prominent as earlier in the day, as the updrafts begin to meander slightly. The meandering of the updrafts is accompanied by the formation of smaller, more intense downdrafts than the broad, weak downdrafts seen earlier in the day, e.g. at 35° 47’ S, 145° 56’ E. The effect of these downdrafts is seen at the surface where divergence of the wind streamlines increases. At 1500 EDT, the mixed layer depth has increased to 4.0 km and the plan view of the boundary-layer rolls reveals that they have become less regular, taking on the pearls on a string appearance seen in the satellite imagery (Figure 3.5).

3.1.3 Potential effect on fire danger

As mentioned in Section 2.1, this case study considers boundary-layer rolls that occurred on the afternoon of Black Saturday, a day of catastrophic fires across the State of Victoria. In order to estimate the potential effect that the boundary-layer rolls have on fire danger in our area of study, we calculate the McArthur Forest-Fire Danger Index (FFDI) using the instantaneous output from our simulations. The FFDI is a commonly used means of assessing the potential danger posed by fire in Australia according to the meteorological conditions and fuel availability. Although the FFDI was originally designed to be calculated daily, to provide an indication of the maximum fire danger on a given day, this type of calculation using instantaneous data does provide a useful guide to how fire danger varies spatially and through the course of the day. The FFDI is calculated using

$$\mathrm{FFDI} = 2\exp[-0.45 + 0.987\ln(\mathrm{DF}) - 0.0345\,\mathrm{RH} + 0.0338\,\mathrm{T} + 0.0234\,\mathrm{V}], \quad (1)$$

after Noble et al. (1980), where DF is the drought factor, RH the relative humidity (%), T the temperature (°C) and V the wind speed (km h^{-1}). The drought factor represents the fuel availability and is a function of the soil-moisture deficit and recent rainfall (Griffiths 1999).

Figure 3.9 shows the FFDI in the area of study throughout the afternoon of 7 February 2009 calculated from instantaneous meteorological output from the 400-m domain and using a drought factor of 10.0, the daily value for the area of study, taken from the dataset of Dowdy et al. (2010).

At 1245 EDT there is a clear spatial pattern to the FFDI, characterised by stripes of relatively low FFDI imposed on a steady background value of about 70. By comparing this pattern to Figure 3.8, it is clear that the spatial variation is linked to the development of the boundary-layer rolls. The stripes of relatively low FFDI are located directly underneath the updraft portion of the rolls, in the convergence zone where the surface wind speeds are slower than the area average. By 1330 EDT the surface wind speed and temperature have increased, leading to an increase in the average FFDI over the area of study. The intensification, deepening and associated broadening of the boundary-layer roll circulation also lead to an increase in the spacing between the stripes of relatively low FFDI. By far the main contributor to the variation in FFDI is the wind speed. Plots of the individual components of the FFDI (not shown) reveal that (i) the relative humidity varies very little over the area of study, (ii) the reduced wind speed below the updrafts is the cause of the stripes of low FFDI and (iii) the temperature, being warmer beneath the updrafts, is actually anti-correlated with the FFDI variations, but the wind variability is so large as to obscure the smaller temperature effect.

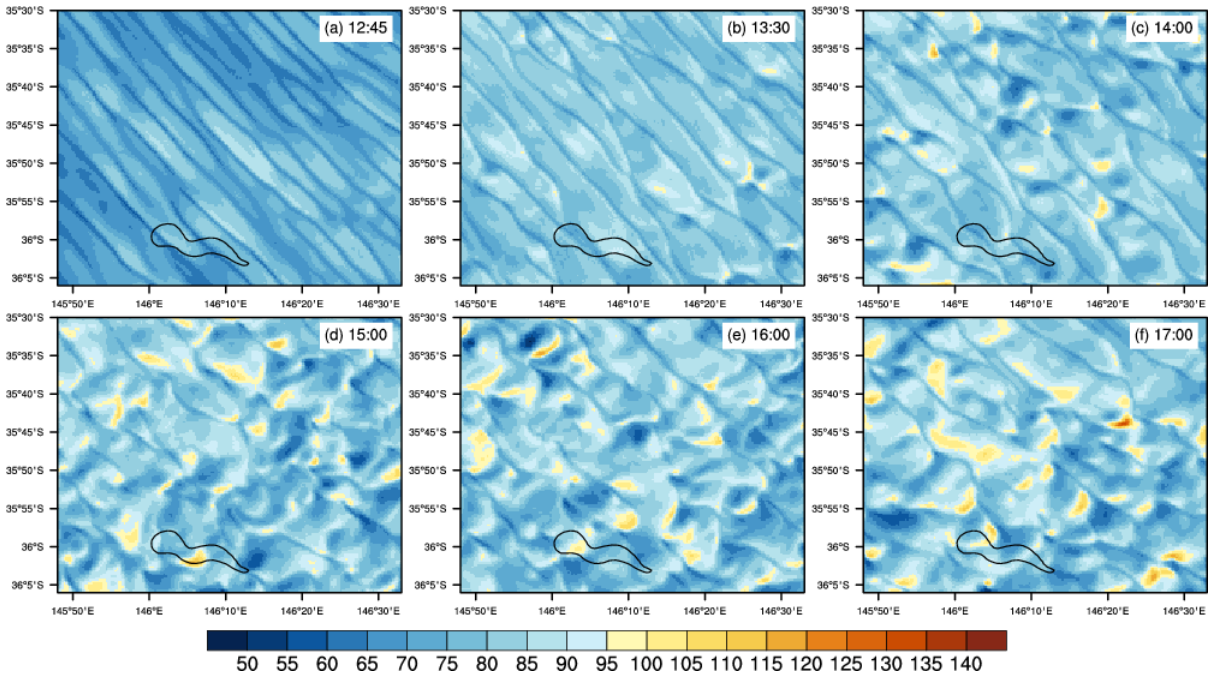

Figure 3.9: FFDI calculated from instantaneous output of the 0.004° simulation at (a) 1245, (b) 1330, (c) 1400, (d) 1500, (e) 1600 and (f) 1700 EDT, on 7 February 2009 and using a drought factor of 10.0.

The nature of the FFDI spatial variability has begun to change by 1400 EDT. Although the pattern is still dominated by stripes of relatively low FFDI imposed on a higher background field, small patches of increased FFDI are also beginning to appear. The timing of this transition coincides with the rolls beginning to meander and their linearity decreasing. As identified in Figure 3.8c, the broad, weak downdraft arms of the circulations become augmented by smaller and more intense downdrafts as the rolls begin to meander. More patches of elevated FFDI can be seen by 1500 EDT, when the rolls were identified to have taken on the "pearls on a string" appearance. If we examine the specific patch of elevated FFDI centred at 35° 57' S, 145° 56' E in Figure 3.9d in conjunction with the plan view of vertical velocity and surface streamlines for the same time, shown in Figure 3.8d, it is clear that the elevated FFDI is located at the downwind edge of a downdraft. As the downdraft impacts upon the surface its downward vertical momentum is transferred horizontally (similar to the outward splash when a bucket of water is tipped on to the floor). This leads to an increase in local divergence and an acceleration of the horizontal surface wind downstream of the downdraft, which is responsible for the patch of elevated FFDI. The transition of the FFDI variability from stripes of

relatively low FFDI to patches of relatively high FFDI continues through 1600 and 1700 EDT as the linearity of the boundary-layer rolls continues to decrease. This transition has implications for the potential fire danger, with the downdraft-related patches resulting in FFDI values raised from 60 to 120 over the space of a few kilometres. These local increases in FFDI equate to raising the fire danger rating two categories, from “severe” (50–75) to “catastrophic (code red)” (> 100). This is a far more serious situation for local fire danger than the negative FFDI anomalies seen earlier in the afternoon.

This study shows that boundary-layer rolls are well represented in the high-resolution model runs. Indeed boundary-layer rolls were also present in some coarser resolution experimental domains, but they developed later and persisted for longer. These experiments showed that a grid spacing of about 600 m or less was required to resolve the boundary-layer rolls secondary circulation and thus accurately reproduce their onset, scale and evolution. However, the horizontal scale of the boundary-layer roll secondary circulation is somewhat dependent on the depth of the boundary layer, which was particularly deep on Black Saturday (about 5 km). Boundary-layer rolls more typically occur in shallower boundary layers with correspondingly more compact secondary circulations, which would require smaller grid spacing to adequately resolve. The study was one of the first to adequately simulate boundary-layer rolls in an operational NWP system (run at very high resolution in research mode). However, the success was due to the high resolution, which is not computationally possible for operational NWP forecasts at present.

The fire-danger implications of the boundary-layer rolls include spatial variation in wind speed and direction on a time scale of 10-15 minutes. Such wind variability can increase the fire spread rate, by broadening the fire head. It also leads to alternating acceleration and deceleration of the fire flanks as the wind component in the direction of the flanks increases and decreases, which can potentially be quite dangerous for fire crews working the fire flanks. Another fire-danger implication is the

potential for enhanced ember transport and associated spotting. We found that the updraft branches of the boundary-layer rolls were narrower and more intense than the downdraft branch, with peak updrafts in excess of 7 m s^{-1}.We hypothesise that the rolls may have contributed to long-range spotting, in which the fire plume lofts the embers to a height of at least 1 km, where the roll circulation is sufficient to support them. Here, the confluence of the flow into the lower part of the rolls may assist in concentrating embers into the updrafts. Once in the updraft, the embers are transported by the strong winds aloft, until eventually they fall.

3.2 Large Eddy Model results

3.2.1 Wind impact on Fire Plume Study

Perhaps surprisingly the wind influence on fire plume structure is not well understood, with only qualitative relationships between some wind regimes and plume structure having been identified in observational and modelling studies. A quantitative relationship has been elusive due to difficulties in observing fire plumes and the very wide range of potential plume structures and behaviours associated with a seemingly infinite range of possible wind and atmospheric stability regimes. This is further complicated by additional variables such as humidity, terrain, fuel types, fire size and fire intensity. An early theoretical study by Byram (1959) attempted to quantify plume behaviour based on a simple energetics argument that pitted plume energy against wind energy to separate the plume into one of two categories. Subsequent field studies have failed to support the theory (e.g., Sullivan 2007), perhaps because the model was too simplistic. In recent times computing power has enabled realistic plume modelling and the potential to perform hundreds or even thousands of simulations to establish a plume structure and behaviour climatology as a function of background wind. However, prior to this project very few experiments have been performed. Of these none have focused on lofting potential, and none have been performed in what we believe to be a realistic turbulent boundary layer. This field of research is very young and provides a great opportunity for important and highly valuable work.

As discussed in Section 2.2 the LEM is run for a few hours before the plume is added in order to spin up a realistic turbulent boundary layer. A plan view of the 800 m vertical velocity for the 15 m s^{-1} wind case is shown in Figure 3.10 to give an indication of the scale and magnitude of the eddies resolved in these LEM simulations.

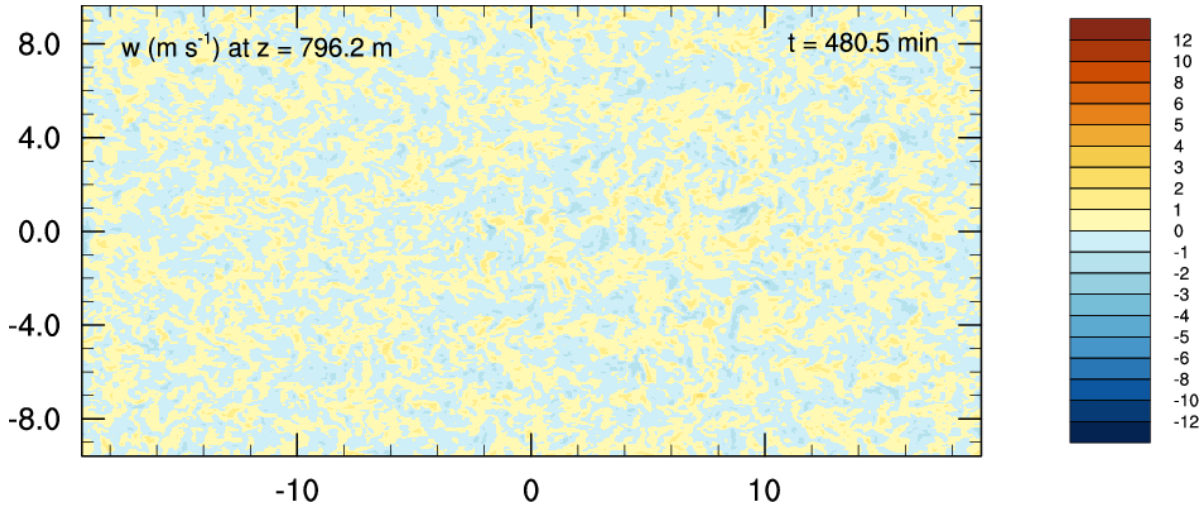

Figure 3.10: Vertical velocity (m s^{-1}) after 8 hours simulation on the 800 m surface, from the 15 m s^{-1} wind case.

An idealised bushfire plume is introduced into the simulations using a methodology similar to that of Devenish and Edwards (2009). A circular heat flux anomaly, of radius 250 m and intensity 100 kW m^{-2}, is situated at the model's lower boundary, 2 km from the upwind boundary in the *x*-direction and equidistant from the lateral boundaries in the *y*-direction. It is to be noted that there is no direct feedback of the atmosphere back onto the fire in these simulations and therefore no capacity to investigate fire spread. Therefore, in this configuration it is possible to isolate and study just the interaction between the plume and background conditions, without the extra complication of the surface-fire behaviour. The idealised surface "fire" is applied to all six background wind-speed simulations and it is found that in each case, the resultant plume reaches a quasi-steady state after 30 minutes of integration time. The simulations are then integrated for a further 60 minutes to

collect statistics of the "mean" plume behaviour, as well as instantaneous model output. Here, we first examine snapshots of the plume under the weakest (2 m s^{-1}) and strongest (15 m s^{-1}) background winds, to illustrate the plume behaviour under different regimes, before considering the "mean" plume behaviour for all wind conditions.

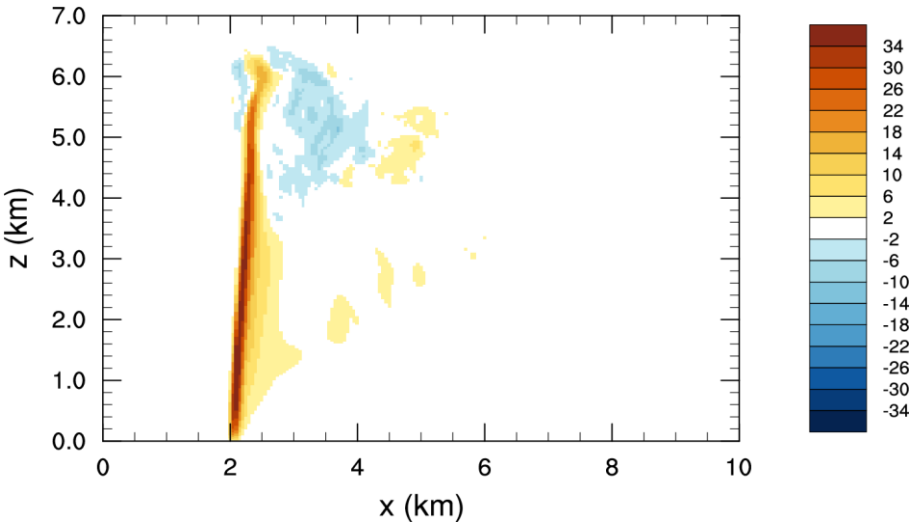

Figure 3.11: Snapshot of the instantaneous centreline vertical velocity, m s^{-1}, after 30 minutes of model time in the 2 m s^{-1} background-wind simulation.

A snapshot of the instantaneous vertical velocity through the plume's centreline after 30 minutes of model time in the 2 m s^{-1} background-wind simulation is shown in Figure 3.11. The updraft is very narrow and also very intense, with peak vertical velocities in excess of 40 m s^{-1}. The plume is nearly vertically aligned and overshoots the top of the mixed layer by a height of more than 3 km. Animation of the plume, not shown, reveals that the location of the plume is very steady, except in the region above the mixed layer, where there is some weak meandering as the plume decelerates. This behaviour is consistent with the weak turbulence of the background wind in this case.

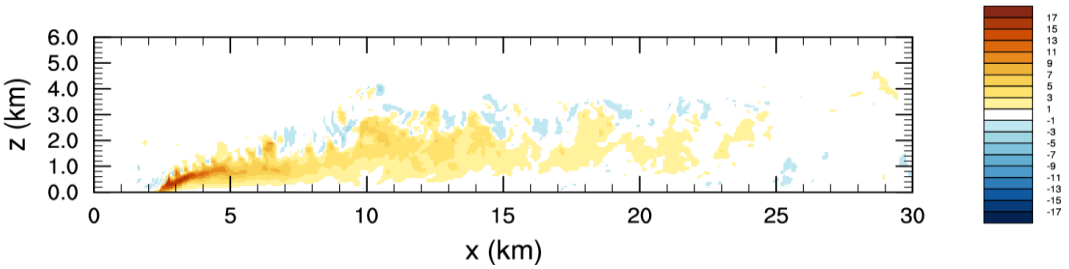

Figure 3.12: Snapshot of the instantaneous centreline vertical velocity, m s^{-1}, after 30 minutes of model time in the 15 m s^{-1} background-wind simulation.

The instantaneous vertical velocity snapshot of the plume with a 15 m s^{-1} background-wind (Figure 3.12) reveals substantially different behaviour of the plume under strong winds. In contrast to the 2 m s^{-1} background-wind case, the plume is very broad and bent over. It is much less intense, with a peak updraft of just over 16 m s^{-1}, and does not extend beyond the top of the mixed layer. Animation of the plume, reveals that the plume is very turbulent, exhibiting strong meandering and pulsing, despite the lack of direct feedback of the atmosphere onto the fire.

The properties of the "mean" plume for each background windspeed, calculated from 60 minutes of model integration in each case, is shown in Figure 3.13. The maximum time-averaged updraft strength (Figure 3.13a) is found to vary smoothly from 41 m s^{-1} under a background windspeed of 2 m s^{-1} to 11 m s^{-1} under a background windspeed of 15 m s^{-1}. The maximum updraft alone is not necessarily a useful predictor for firebrand transport, so we also plot contours of the 6 m s^{-1} updraft along the domain centre line for each background windspeed (Figure 3.13b). We chose this contour level as it is representative of a typical firebrand fall velocity (e.g., Ellis 2010).

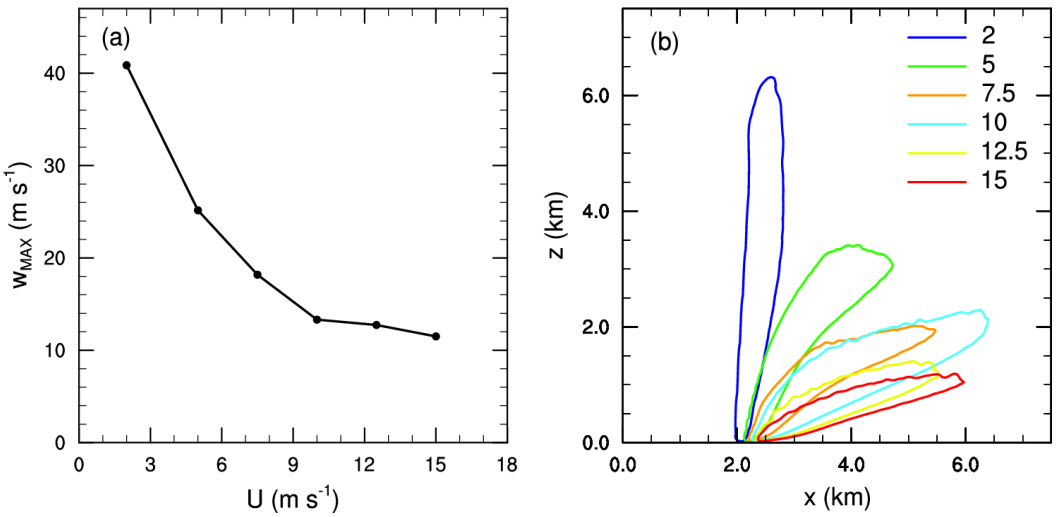

Figure 3.13: Properties of the plumes time averaged over one hour at quasi-steady state. (a) Maximum updraft speed, m s^{-1}, as a function of background windspeed, m s^{-1}; and (b) location of the 6 m s^{-1} updraft contour along the domain centre line for each of the six background windspeed simulations.

Here we can see that although under weak wind conditions the peak updrafts are of the order four times larger than under strong wind conditions, the area of each individual plume that contains an updraft strong enough to suspend a typical firebrand is actually quite comparable.

Estimates of the downstream firebrand transport can be obtained using Figure 6b. Using a fall speed of 6 m s^{-1}, representative of large firebrands, and taking the downstream location of the greatest height of the 6 m s^{-1} updraft contour, and factoring in a 6 m s^{-1} descent at the background horizontal wind speed, we get firebrand transport distances of about a 2.5, 7.5, and 6.5 km for the 2, 10 and 15 m s^{-1} background wind cases respectively. Using this simple argument firebrands in the lighter wind environments are lofted deeper so they might spend more time aloft, but the downstream advection is weaker. The ideal combination of lofting depth and downstream advection speed for maximum transport distance appears to be for the 10 m s^{-1} background wind case. In reality a broad distribution of firebrand transport from each plume would be expected. A Lagrangian transport model is currently under construction to calculate a more realistic firebrand transport distribution.

Snapshots of instantaneous tracer concentration isosurfaces, after the plumes have reached a quasi-steady state are shown in Figure 3.14 for the 15 and 5 m s^{-1} background wind cases. In the stronger background wind case the plume is meandering and turbulent all the way from the surface up to its maximum height. In the weaker background wind case, the plumes tracer isosurface is much smoother in the lower half, consistent with the near-laminar flow observation made above, before becoming turbulent in the upper half of the plume. These turbulent structures are well documented. They result from shear instability due to the strong gradient in wind speed at the plume edge. An excellent illustrative example of this process is evident in Figure 2b of Fric and Roshko (1994) reproduced here as Figure 3.15. Fric and Roshko (1994) also document the pair of counter-rotating vortices evident in the lower half of the 5 m s^{-1} plume case (Figure 3.14).

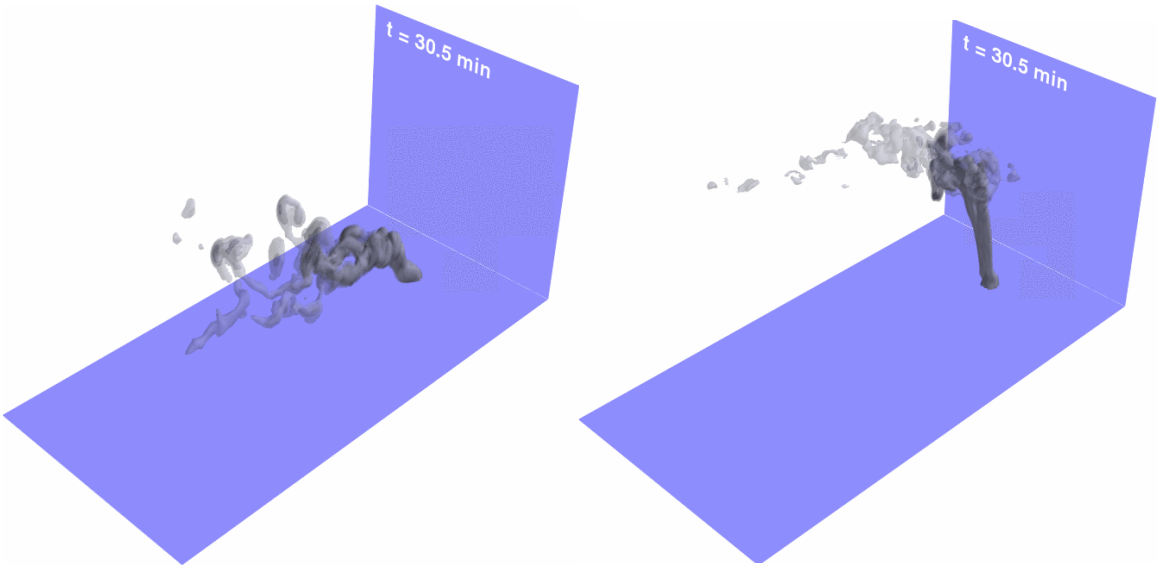

Figure 3.14: Snapshots of instantaneous concentration of a passive tracer released at a constant rate from the surface over the area representing the fire, for the 15 m s^{-1} (left panel) and 5 m s^{-1} (right panel) background wind cases.

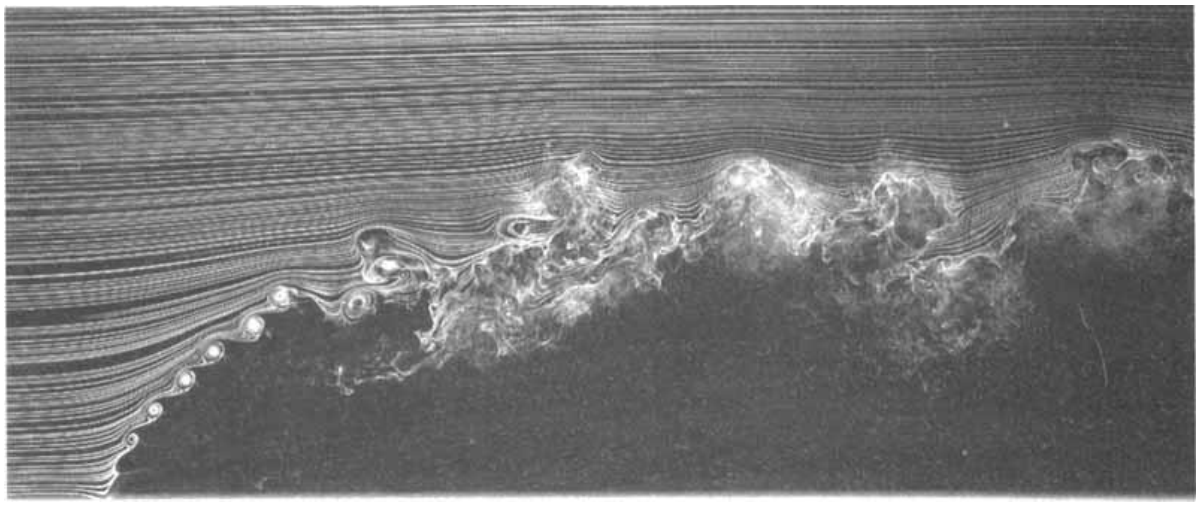

Figure 3.15: Transverse-jet shear-layer structure visualized by smoke streamlines entrained into the leading edge of the jet. The image is similar to a vertical cross-section through the centre line of the LEM plumes. Image from Figure 2b of Fric and Roshko (1994).

3.2.2 Boundary-layer roll impact on fire plume study – LEM

In the final part of the project we departed from the systematic approach to investigating wind influence on plume behaviour and structure. In order to tie the first two components of the project together we chose to investigate the specific case of boundary-layer roll influence on plume

behaviour by introducing conditions conducive to boundary layer roll development to the LEM, and then adding two plumes (in separate experiments): one plume to a region of updraft and one plume to a region of downdraft. Before analysing the plume cases we document the boundary-layer rolls without plumes, as follows.

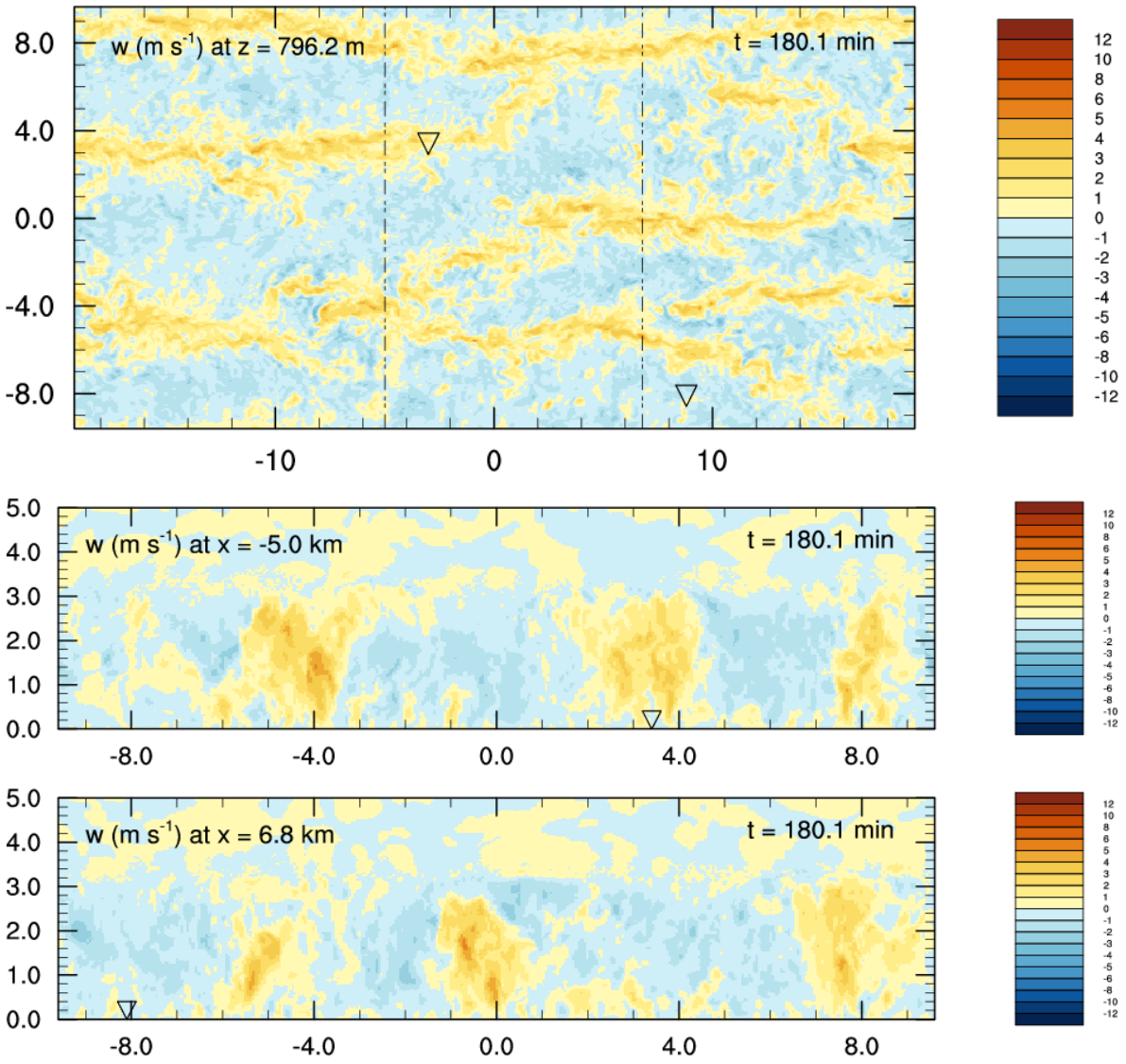

Figure 3.16: Vertical velocity (shaded, in m s^{-1}) from the LEM boundary layer roll simulation after three hours of model spin-up. Upper panel, horizontal section 800 m above the surface. The dashed lines indicate the position of two vertical cross sections featured in the middle (left-most dashed line) and lower panels (right-most dashed line), which are located upstream of the two plume locations, indicated by the triangles. (The left edges of the vertical panels coincide with the lower edge of the horizontal panel.) The horizontal and vertical distances are in km.

Boundary-layer rolls were initiated in the 15 m s^{-1} background wind simulations after a constant surface heat flux of 50 W m^{-2} was added to provide the necessary thermal instability. Figure 3.16

shows a snapshot of the vertical velocity after three hours of model spin-up. The approximately east-west-oriented linear features in yellow represent the relatively narrow updrafts, with broader regions of descent in blue. The figure also hints at the meandering nature of the rolls, which is evident in time animations. A total of three experiments are reported on here, initialized with the wind structure featured in Figure 8, and run for a further 60 minutes: A control experiment with no plume, and two experiments with plumes. The plumes were added near the coordinates (X,Y) = (0,4) km, and (X,Y) = (10,–8) km in ascending (Figure 3.16, middle panel) and descending (Figure 3.16, lower panel) branches of boundary-layer rolls, respectively.

Figure 3.17 shows the same horizontal cross-section of the vertical wind field but 15 minutes later for all three experiments. Here and in subsequent figures the control wind field is placed between the two plume cases for ease of comparison. The plume embedded in the updraft is concentrated and intense, whereas the plume in the downdraft is less intense, more spread-out, and more puff-like, which suggests the roll updraft and associated low-level convergence helps to maintain the plume continuity, and the divergent descending region perhaps contributes to a horizontal plume spread. Also of interest is an apparent vertical mass-flux conservation in the vicinity of the plumes. For example, a comparison of the intensity of the vertical motion to the north and south of the plume in the ascent region with the no plume case, shows in the former a more intense downdraft to the north and weaker updraft to the south. Similarly the plume in the descent region is surrounded by regions of enhanced descent compared with the no-plume case. This suggests that the dynamic forcing governing the boundary layer roll vertical mass flux is quite strong.

The difference in plume structure is further evident in the vertical cross-sections through the two plumes at the same time in Figure 3.18, which also includes a similar section through the 15 m s^{-1} background wind plume described in Section 3.2.1 (without the boundary-layer rolls). The plume embedded in the boundary layer roll ascent region (Figure 3.18 upper panel) is noticeably deeper,

and more intense than the case with no boundary-layer rolls (Figure 3.18 middle panel), which in turn is a little deeper and a little more intense than the plume in the boundary layer roll descent region (Figure 3.18 lower panel). This latter plume appears to have larger puff-like structure as well, which was also evident in Figure 3.17.

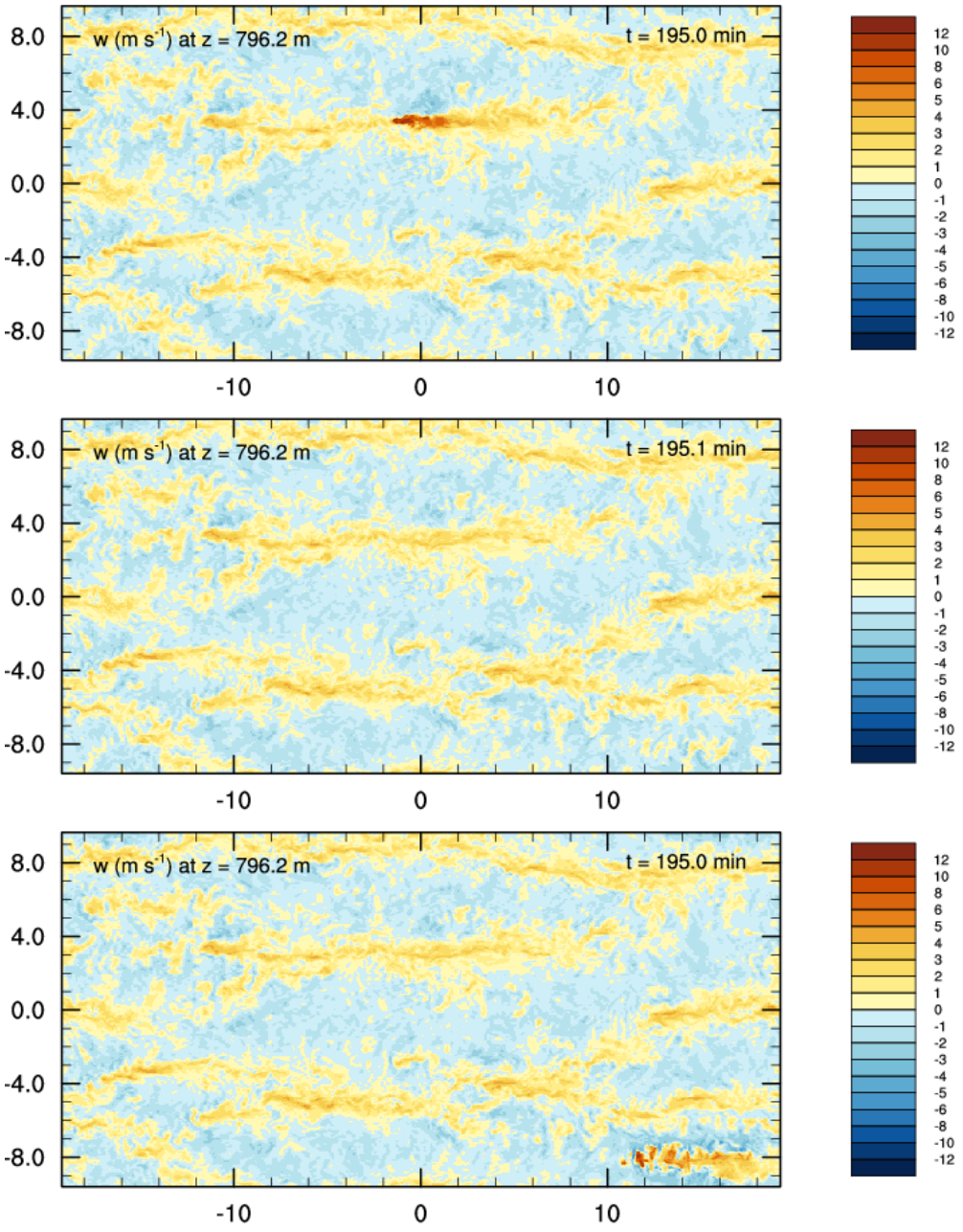

Figure 3.17: Same as the top panel of Figure 3.16 except 15 minutes later, for three experiments with the plume in a boundary-layer roll ascending region (upper panel, (X,Y) = (–2.0,3.4) km), the control (no-plume, middle panel) and the plume in a boundary-layer roll descending region (lower panel, (X,Y) = (10.0, –8.1) km). In these plots the abscissa and ordinate represent the X- and Y-directions respectively.

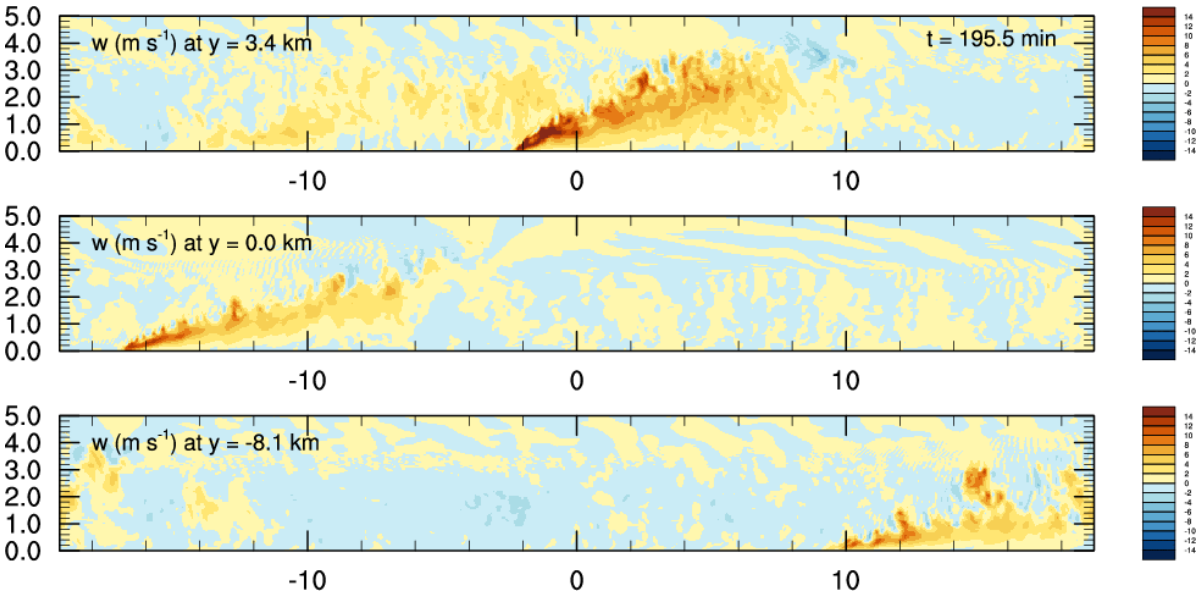

Figure 3.18: Vertical cross-sections through the plume centres 15 minutes after the heat source was added for (upper panel) the plume in the ascending branch of the boundary-layer roll (c.f., Figure 3.17 upper panel), (middle panel) the 15 m s^{-1} wind case (no boundary-layer rolls, 15 minutes earlier than that shown in Figure 3.12), and (lower panel) the plume in the descending branch of the boundary-layer roll (c.f., Figure 3.17 lower panel).

Another thirty minutes later the first plume has become located in a region of descent (Figure 3.19), as a result of the meandering rolls. It is now broader, more puff-like and less intense. Interestingly, at this time the plume originally embedded in a boundary-layer roll descending branch is entering a region of weak ascent. In comparison with the plume structure from 30 minutes earlier the former descent plume is beginning to look more coherent. Vertical cross sections at this later time are presented in Figure 3.20. The first plume is visibly less intense than it was 30 minutes earlier (upper panel), and is now confined below a depth of 1000 m for about 1.5 km downstream of the plume source. It is more depressed than the case with no boundary-layer rolls also (middle panel). The plume originally located in the descent branch is just beginning to become more vertical (lower panel) as it is engulfed by a region of ascending flow (pale yellow shading). The changing plume suppression and enhancement is particularly evident in animations of the simulations.

These results suggest the relationship between coherent intense plumes in ascending boundary-layer roll branches and weaker more laterally spread and puff-like plumes in descending branches, is quite robust.

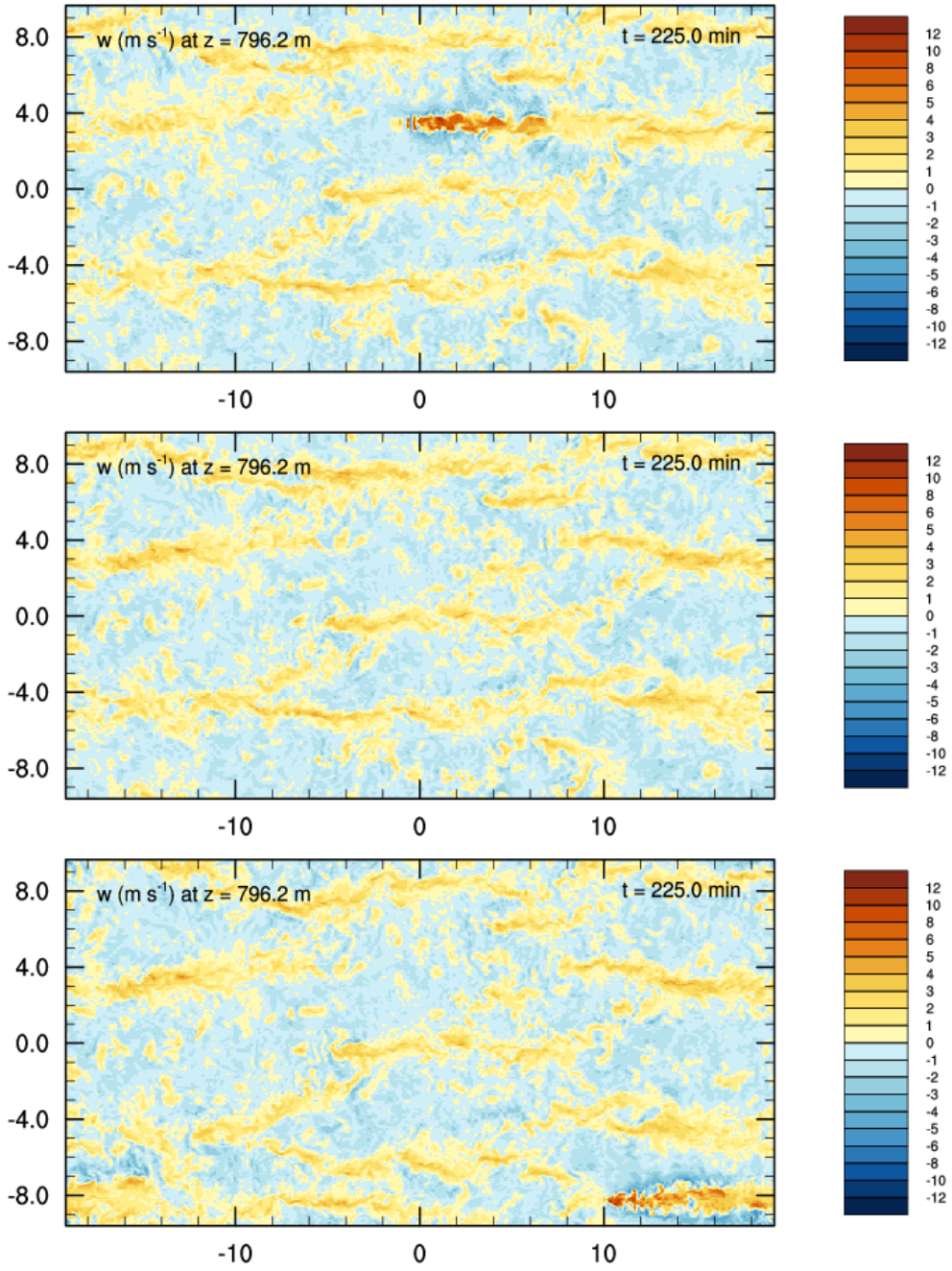

Figure 3.19: Same as Figure 3.17 but thirty minutes later (3 hours 45 minutes into the simulation).

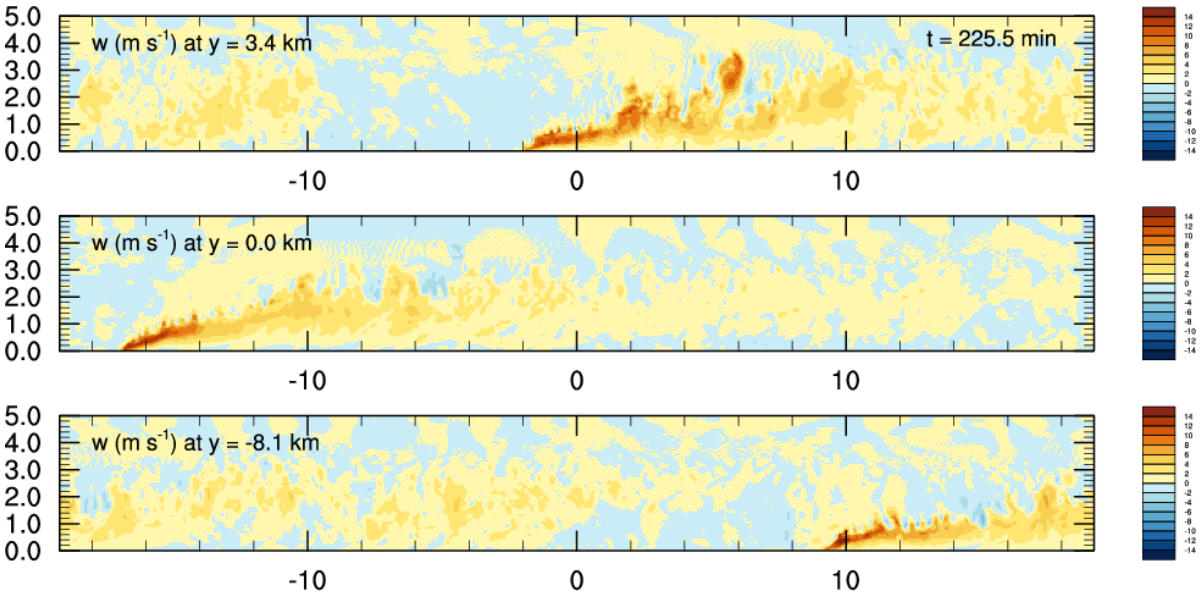

Figure 3.20: Same as Figure 3.18 but thirty minutes later (45 minutes after the plume heat source was added).

While these results are particularly interesting and of great importance for understanding plume behaviour in variable wind regimes, it is important to remember that the simple Idealised studies include no fire-atmosphere feedback. While the plumes appear to be deeper and more intense when embedded in a region of ascent, and weaker and shallower when in a region of descent, one might expect an associated enhanced low-level convergence and divergence respectively that further enhances and suppresses the fire respectively. This will be investigated in the near future. However, it is quite possible that non-linear affects could lead to much less predictable fire burn and spread rates, especially if there are sudden changes in ascent and descent in the fire vicinity.

4 Discussion: Relevance to people on the fireground

4.1 ACCESS Boundary-layer rolls

The boundary-layer rolls comprised of a sequence of counter-rotating horizontal vortices aligned approximately with the mean wind direction and had meandering quasi-linear updrafts in excess of 5 m s^{-1}. We expect that these may have contributed to ember transport during Black Saturday. They also led to significant fluctuations in near-surface wind speed and direction, as well as temperature (and humidity to a somewhat lesser degree), on a time-scale of the order of 10 minutes, which would have likely influenced fire burn rate and spread rate. The variation in wind direction is perhaps especially significant, since it would have helped the fire front to broaden, leading to a more intense and faster-moving fire, and the variations in wind speed would have a dominant role in influencing fire weather conditions as represented by indices such as the FFDI. The structure evident in the plan view and cross-sections of the modelled boundary-layer rolls (Figure 3.8) is confirmed by radar and satellite data. As time progressed, daytime heating caused the boundary layer to deepen, and hence the rolls to deepen and broaden. The character of the rolls also changed, with them becoming less linear and eventually breaking up into cellular convection.

The fire-danger implications of the boundary-layer rolls associated with the spatial variation in wind speed and direction (on a time scale of 10-15 minutes), not only increases the fire spread rate, by broadening the fire head, but it can also lead to alternating acceleration and deceleration of the fire flanks as the wind component in the direction of the flanks increases and decreases. This aspect of wind variability can potentially be quite dangerous for fire crews working the fire flanks.

Another fire-danger implication is the potential for enhanced ember transport and associated spotting. We found that the updraft branches of the boundary-layer rolls were narrower and more

intense than the downdraft branch, with peak updrafts in excess of 7 m s^{-1}. We hypothesise that the rolls may have contributed to long-range spotting, in which the fire plume lofts the embers to a height of at least 1 km, where the roll circulation is sufficient to support them. Here, the confluence of the flow into the lower part of the rolls may assist in concentrating embers into the updrafts. Once in the updraft, the embers are transported by the strong winds aloft, until eventually they fall.

The instantaneous forest fire danger index (FFDI) was also found to vary considerably across the ascending and descending branches of the boundary-layer rolls, with more extreme values appearing as the rolls began to transition to more cellular convection. This transition has obvious implications for the potential fire danger, with the downdraft-related patches resulting in FFDI values raised from 60 to 120 over the space of a few kilometres. These local increases in FFDI equate to raising the fire danger rating two categories, from “severe” (50–75) to “catastrophic (code red)” (> 100). This is a far more serious situation for local fire danger than the negative FFDI anomalies seen earlier in the afternoon. This result of extreme FFDI in the descent regions should be contrasted with the plume studies that found the plumes were most intense in the ascending branches of the boundary-layer rolls.

4.2 Large Eddy Model Plume response to wind speed

The plumes subsequently simulated across a range of windspeeds (2 to 15 m s^{-1}) displayed markedly different behaviour. Under weak background winds, plumes were intense, narrow, upright and smooth, whereas under strong background winds the plumes were comparatively weak, broad, bent over and turbulent. However, all plumes contained substantial areas of updrafts that would be sufficiently strong to suspend a typical firebrand. Despite a wide variation in plume structure across the wind speed regimes, all plumes showed considerable potential for firebrand lofting. Using a fall

speed of 6 m s^{-1}, representative of large firebrands, the 2 m s^{-1} background wind case demonstrated the potential to loft 6 km vertically, but perhaps only 500 m downstream. Falling at 6 m s^{-1} it would take about 17 minutes for the firebrand to reach the ground, which, in a background wind of 2 m s^{-1}, would lead to another 2 km downstream transport for a total horizontal transport of 2.5 km. In contrast the 15 m s^{-1} background wind case could loft 1 km vertically and about 4 km downstream before the firebrand would begin to descend, which would be followed by about another 2.5 km downstream transport, giving a total of 6.5 km horizontal transport. An optimum combination for downstream transport appeared to be the 10 m s^{-1} background wind case, which could loft the firebrand 2 km vertically and about 4 km downwind, before it would begin to descend. During its descent it would travel another 3.3 km, giving a total of 7.3 km horizontal transport. These transport distances are based on very simple assumptions about firebrand lofting and descent. In reality a broad distribution of firebrand transport would be expected. A Lagrangian transport model is currently under construction to calculate a more realistic firebrand transport distribution. However, neither method considers the increasing firebrand burn-out rate as a function of time aloft.

It follows that more complex background wind scenarios of light winds near the surface and stronger winds aloft for example, could potentially have greater potential for horizontal firebrand transport. The addition of moisture to the model, could further enhance lofting and horizontal transport potential if additional buoyancy was added to the plume through condensational heating, and subsequent pyrocumulus development. Plume depth will also vary with dry atmospheric stability and the intensity and size of the parameterised fire heat source. Sensitivity to these variables will be investigated in future work.

Although the idealised fire prescribed here was relatively intense and simulated under a wide range of wind conditions, the simple firebrand transport arguments above suggest the plumes simulated

here would unlikely be strong enough to give rise to long-range spotting such as that observed during Black Saturday (in excess of 30 km, Cruz et al. 2012). One potential reason for this is the lack of any moisture in either the fire or atmosphere, which is thought to play an important role in the dynamics of real-world fire plumes, particularly through the formation of pyrocumulonimbi (e.g., Cunningham and Reeder 2009).

4.3 Large Eddy Model – Plume response to boundary-layer rolls

The previous two components of the study showed that the idealised plume for all wind regimes could easily loft burning embers more than 1 km above the surface, and that the boundary-layer rolls contained updrafts strong enough to loft burning embers from about 1 km above the surface and beyond. This gave rise to our hypothesis that boundary-layer rolls could contribute to ember transport once the fire plume first lofted the embers to about one km or higher above the surface. The Idealised plume plus boundary-layer roll experiment using the LEM showed significant enhancement in the plume depth and intensity when located in an ascending branch of the boundary-layer rolls, and the opposite was observed in the descending branches, with shallower, weaker and broader, more puff-like plumes. The former behaviour is similar to descriptions of Byram's (1959)"plume-driven" fires, and the latter his "wind-driven" fires, with the former associated with extreme fire behaviour. It follows that this simple, preliminary experiment may have identified a mechanism for rapid change in fire behaviour. It is possible that the difference in associated fire behaviour in a real fire may be more extreme if the more intense updraft leads to enhanced low-level convergence that increases the burn rate. This mechanism is not necessarily restricted to boundary-layer rolls. Similar behaviour might be expected with any meteorological feature associated with a concentrated region of low-level ascent (e.g., sea-breeze fronts, sea-breeze convergence lines, wind changes, cold fronts, solitary waves, c.f., Peace et al. 2012). This changing plume behaviour with background vertical wind flow, is consistent with the considerable

anecdotal evidence of extreme fire behaviour in south eastern Australia with the passage of wind changes.

5 Summary

Almost every result from the LEM studies has contributed to an advancement of the state of knowledge of plume behaviour in a realistic turbulent boundary layer. We now know that an intense heat source in a low-wind speed environment generates a deep, intense and coherent plume that can penetrate many kilometres into the stable layer above the well mixed boundary layer, with updraft speeds in excess of 20 m s^{-1}. It follows that entrainment into such a plume must be minimal for it to remain buoyant to such a great depth. With increasing wind speeds, the plume becomes shallower, less intense, more bent over and increasingly more puff-like. The higher wind speeds advect the plume downwind, leading to the bent-over appearance. We expect the increasing energy of the turbulence in the higher wind cases facilitates greater entrainment, which reduces the plume buoyancy and also encourages the breakdown of the plume into buoyant puffs, leading to very realistic-looking bushfire-like smoke behaviour.

We now know that an intense circular heat source of 100 kW m^{-2} over a radius of 250 m will generate updraft speeds capable of lofting large firebrands (with fall velocities up to 6 m s^{-1}) more than 1 km deep for all background wind speeds up to at least 15 m s^{-1}. Indeed, if a fire is capable of burning at that intensity in a background wind environment of 2 m s^{-1}, lofting to 6 km deep (in an environment of typical tropospheric stability) without any contribution to plume buoyancy from condensational heating seems quite plausible.

This project has revealed that plume behaviour in a strong background wind environment (15 m s^{-1}) can be particularly sensitive to environmental ascent and descent in the immediate vicinity of the plume. In a relatively weakly ascending region the plume becomes more upright, and very much more concentrated and coherent, with an almost doubling of the plume height. We suspect the

more rapid ascent reduces the time for entrainment to dilute the plume buoyancy, and reduces the downstream plume advection and thus the tendency to break the plume into buoyant puffs. On the other hand the weaker, more bent-over and spread-out plumes in the descent regions, are advected further downstream which is likely to favour the plume break-down into buoyant puffs as the plume is stretched out horizontally. The greater surface area of the plume and puffs is expected to enhance entrainment of cooler environmental air, which will further dilute the plume and puff buoyancy. If the plume and puff entrainment is governed to a large extent by the surface area and exposure time, we hypothesise a positive feedback in which a plume that is suppressed by environmental descent will spend more time entraining cooler environmental air. The greater buoyancy dilution rate will lead to a greater reduction in upward plume and puff acceleration, resulting in greater entrainment and plume and puff deceleration. The opposite will be true for a plume in a region of ascent. With respect to dangerous plume behaviour, these results suggest regions of ascent are likely to be particularly hazardous, because they contribute to firebrand lofting, and they strengthen the plume.

While this plume behaviour was identified in a simulation in which boundary-layer rolls provided the vertical flow, the lessons learned suggest any meteorological phenomena that produces local ascent should be of concern. This includes wind changes associated with trough lines, cold fronts, sea breezes, and solitary waves such as the undular bore observed during Black Saturday. It also includes the ascending branches of dry cellular convection, and especially moist convection. Pyrocumulus is potentially an extreme example when the moist ascent region can become attached to the plume itself. These conclusions are consistent with many studies and considerable anecdotal evidence of unexpected extreme fire behaviour.

The boundary-layer roll ACCESS modelling study largely confirmed suspected wind behaviour known to influence fire spread rates: horizontal wind direction variability, and ascent and descent associated with the vertical circulation. What was surprising was the large extent of the periodic wind direction variability (60°) and the strength of the maximum updraft (> 8 m s^{-1}). These results together with the plume study suggest boundary-layer rolls could contribute to more destructive fire behaviour than previously thought, with the wind direction variability contributing to a broader and faster moving fire front, and the updrafts contributing to enhanced lofting potential, and an intensification of the plume. Additionally the greatest FFDI was found to be located in the descent region, which potentially could partly offset or override the effect of the suppressed plume found in regions of descent.

Acknowledgements

We would like to thank the many people who reviewed the numerous papers, reports, briefing notes, conference abstracts and posters, throughout the entirety of the project: Andrew Dowdy, Chris Lucas, Claire Yeo, Graham Mills, Mika Peace, Yimin Ma and Dale Hess. Thanks also to Andrew Sullivan, Peter Ellis and Simon Haemstra for very useful and informative discussions. Lastly, we'd like to acknowledge the following Bushfire CRC officers for their support and assistance:

Lyndsey Wright, Richard Thornton, Noreen Krusel, David Bruce, Nathan Maddock, Annette Allen, Vaia Smirneos and Kate Twentyman.

References

Andrejczuk M, Grabowski WW, Gadian A, Burton R. 2012. Limited area modelling of stratocumulus over South-Eastern Pacific. *Atmos. Chem. Phys*. **12**, 3511–3526.

Andren, A., A. R. Brown, P. J. Mason, J. Graf, U. Schumann, C.-H. Moeng, and F. T. M. Nieuwstadt (1994). Large-eddy simulation of a neutrally stratified boundary layer: A comparison of four computer code. *Q. J. Roy. Meteor. Soc*. **120**, 1457–1484.

Atkinson BW, Zhang JW. 1996. Mesoscale shallow convection in the atmosphere. *Rev. Geophys*. **34**, 403–431.

Belušić D, Güttler I. 2010. Can mesoscale models reproduce meandering motions? *Q. J. Roy. Meteor. Soc*. **136**, 553–565, doi: 10.1002/qj.606.

BoM. 2008. Long-term rainfall deficiencies continue in southern Australia while wet conditions dominate the north, Bureau of Meteorology, Special Climate Statement 16. *Issued 10th October 2008.*

BoM. 2009a. The exceptional January-February 2009 heatwave in southeastern Australia, Bureau of Meteorology, Special Climate Statement 17. *First Issued 4th February 2009, Updated 12th February 2009*.

BoM. 2009b. Bureau of Meteorology 2009b. Meteorological aspects of the 7 February 2009 Victorian fires, an overview. Bureau of Meteorology, Melbourne, Australia.

Brooks IM, Rogers DP. 1997. Aircraft observations of boundary-layer rolls off the coast of California. *J. Atmos. Sci.* **54**, 1834–1849.

Brown AR, Derbyshire SH, Mason PJ. 1994. Large-eddy simulation of stable atmospheric boundary layers with a revised stochastic subgrid model. *Q. J. Roy. Meteor. Soc*. **120**, 1485–1512.

Brümmer B. 1999. Roll and cell convection in wintertime Arctic cold-air outbreaks. *J. Atmos. Sci*. **56**, 2613–2636.

Byram GM. 1959. Forest fire behavior. In K. P. Davis (Ed.), Forest Fire: Control and Use, pp. 90–123. New York: McGraw-Hill.

Couvreux F, Rio C, Guichard F, Lothon M, Canut G, Bouniol D, Gounou A. 2012. Initiation of daytime local convection in a semi-arid region analysed with high-resolution simulations and AMMA observations. *Q. J. Roy. Meteor. Soc*. **138**, 56–71, doi:10.1002/qj.903.

Cruz MG, Sullivan AL, Gould JS, Sims NC, Bannister AJ, Hollis JJ, Hurley RJ. 2012. Anatomy of a catastrophic wildfire: The Black Saturday Kilmore East fire in Victoria, Australia. *Forest Ecol. Manag*. **284**, 269–285.

Cunningham P, Reeder MJ. 2009. Severe convective storms initiated by intense simulations of pyro-convection and pyro-tornadogenesis. *Geophys. Res. Lett*. **36**, L12812, doi:10.1029/2009GL039262.

Davies T, Cullen MJP, Malcolm AJ, Mawson MH, Staniforth A, White AA, Wood N. 2005. A new dynamical core for the Met Office's global and regional modelling of the atmosphere. *Q. J. Roy. Meteor. Soc*. **131**, 1759–1782.

Devenish B J, Edwards JM. 2009. Large-eddy simulation of the plume generated by the fire at the Buncefield oil depot in December 2005. *Proc. R. Soc.* **A 465**, 397–419.

Dowdy AJ, Mills GA, Finkele K, de Groot W. 2010. Index sensitivity analysis applied to the Canadian Forest Fire Weather Index and the McArthur Forest Fire Danger Index. Meteorol. Appl. 17: 298–312.

Ellis PFM. 2010. The effect of the aerodynamic behaviour of flakes of jarrah and karri bark on their potential as firebrands. *J. Roy. Soc. West. Aust*. **93**, 21–27.

Ellis R, Businger S. 2010. Helical circulations in the typhoon boundary layer. *J. Geophys. Res*. **115**, D06205, doi:10.1029/2009JD011819.

Engel CB, Lane TP, Reeder MJ, Rezny M. 2013. The meteorology of Black Saturday. *Q. J. Roy. Meteor. Soc*. **139**, 585–599.

Etling D, Brown RA. 1993. Roll vortices in the planetary boundary layer: A review. *Bound.-Lay. Meteorol*. **65**, 215–248.

Fawcett RJB, Thurston W, Kepert JD, Tory K. 2013. The meteorology of Black Saturday: a high-resolution ACCESS modelling study. CAWCR Technical Report In preparation, The Centre for Australian Weather and Climate Research, Victoria, Australia.

Fovell RG. 2005. Convective initiation ahead of the sea-breeze front. *Mon. Weather Rev*. **133**, 264–278.

Fric TF, Roshko A. 1994. Vortical structure in the wake of a transverse jet. *J. Fluid Mech.* **279**, 1-47.

Fritts DC, Alexander MJ. 2003. Gravity wave dynamics and effects in the middle atmosphere. *Rev. Geophys*. **41**, 1003, doi:10.1029/ 2001RG000106.

Glendening JW. 1996. Lineal eddy features under strong shear conditions. *J. Atmos. Sci*. **53**, 3430–3449.

Gray MEB, Petch J, Derbyshire SH, Brown AR, Lock AP, Swann HA, Brown PRA. 2001. 'Version 2.3 of the Met Office large eddy model: Part II. Scientific documentation'. Met Office, Exeter, United Kingdom.

Gregory D, Rowntree PR. 1990. A mass flux convection scheme with representation of cloud ensemble characteristics and stability-dependent closure. *Mon. Wea. Rev.*, **118**, 1483–1506.

Griffiths D. 1999. Improved formula for the drought factor in McArthur's forest fire danger meter. *Austral. For*. **62**, 202–206.

Huang Q, Marsham JH, Parker DJ, Tian W, Weckworth T. 2009. A comparison of roll and nonroll convection and the subsequent deepening moist convection: An LEM case study based on SCMS data. *Mon. Weather Rev*. **137**, 350–365, doi:10.1175/2008MWR2450.1.

Kapustin VN, Clarke AD, Howell SG, McNaughton CS, Brekhovskikh VL, Zhou J. 2012. Evaluating primary marine aerosol production and atmospheric roll structures in Hawaii's natural oceanic wind tunnel. *J. Atmos. Ocean. Tech*. **29**, 668–682, doi:10.1175/JTECH-D-11-00079.1.

Kiefer MT, Parker MD, Charney JJ. 2009. Regimes of dry convection above wildfires: Idealised numerical simulations and dimensional analysis. *J. Atmos. Sci*. **66**, 806–836.

Kuettner JP. 1973. Cloud bands in the earth's atmosphere. Observations and theory. *Tellus*, **23**, 404–425.

Lane TP, Clark TL. 2002. Gravity waves generated by the dry convective boundary layer: Two-dimensional scale selection and boundary-layer feedback. *Q. J. Roy. Meteor. Soc*. **128**, 1543–1570.

Liu AQ, Moore GWK, Tsuboki K, Renfrew IA. 2004. A high-resolution simulation of convective roll clouds during a cold-air outbreak. *Geophys. Res. Lett*. **31**, L03101, doi:10.1029/2003GL018530.

Lock AP, Brown AR, Bush MR, Martin GM, Smith RNB. 2000. A New Boundary Layer Mixing Scheme. Part I: Scheme Description and Single-Column Model Tests closure. *Mon. Wea. Rev.*, **128**, 3187–3199.

Mahrt L, 2011. Surface Wind Direction Variability. *J. Appl. Meteorol. Clim.,* **50**, 144–152.

Marsham JH, Parker DJ, Grams CM, Johnson BT, Grey WMF, Ross AN. 2008. Observations of mesoscale and boundary-layer scale circulations affecting dust transport and uplift over the Sahara. *Atmos. Chem.* Phys. **8**, 6979–6993.

Mason PJ, Thomson DJ. 1987. Large-eddy simulations of the neutral-static-stability planetary boundary layer. *Q. J. Roy. Meteor. Soc.* **113**, 413–443.

Mirocha J, Kirkil G, Bou-Zeid E, Chow FK, Kosovic B. 2013. Transition and equilibration of neutral atmospheric boundary layer flow in oneway nested large-eddy simulations using the Weather Research and Forecasting model. *Mon. Weather Rev*. **141**, 918–940.

Moeng C-H, Sullivan PP. 1994.. A comparison of shear- and buoyancy-driven planetary boundary layer flows. *J. Atmos. Sci.* **51**, 999–1022.

Morrison I, Businger S, Marks F, Dodge P, Businger JA. 2005. An observational case for the prevalence of roll vortices in the hurricane boundary layer. *J. Atmos. Sci.* **62**, 2662–2673.

Noble IR, Bary GAV, Gill AM. 1980. McArthur's fire-danger meters expressed as equations. *Aust. J. Ecol.* **5**, 201–203.

Peace M, McCaw L, Mills G. 2012a. Meteorological dynamics in a fire environment; a case study of the Layman prescribed burn in Western Australia. *Aus. Met. Ocean. Journal*, **62**, 127–142.

Price JD, Vosper S, Brown A, Ross A, Clark P, Davies F, Horlacher V, Claxton B, McGregor JR, Hoare JS, Jemmett-Smith B, Sheridan P. 2011. COLPEX: Field and numerical studies over a region of small hills. *B. Am. Meteorol. Soc*. **92**, 1636–1650.

Rothermel RC. 1991. Predicting behavior and size of crown fires in the northern Rocky Mountains. *Research Paper INT-438, USDA Forest Service*, 46 pp., Intermountain Research Station.

Skamarock WC. 2004. Evaluating mesoscale NWP models using kinetic energy spectra. *Mon. Wea. Rev*., **132**, 3019-3032.

Smagorinsky J. 1963. General Circulation Experiments with the Primitive Equations. *Mon. Wea. Rev.*, **91**, 99–164.

Stull RB. 1988. An introduction to boundary layer meteorology. *Kluwer Academic Publishers, Dordrecht*.

Sullivan AL. 2007. Convective Froude number and Byram's energy criterion of Australian experimental grassland fires. *Proc. Combust. Inst*., **31**, 2557–2564.

Sun R, Krueger SK, Jenkins MA, Zulauf MA, Charney JJ. 2009. The importance of fire–atmosphere coupling and boundary-layer turbulence to wildfire spread. *Int. J. Wildland Fire*, **18**, 50–60.

Tang Y, Lean HW, Bornemann J. 2013. The benefits of the Met Office variable resolution NWP model for forecasting convection. *Meteorol. Appl.* doi:10.1002/met.1300.

Tian W, Parker DJ, Kilburn CD. 2003. Observations and numerical simulation of atmospheric cellular convection over mesoscale topography. *Mon. Weather Rev*. **131**, 222–235.

Timbal B. 2009. The continuing decline in South-East Australian rainfall: update to May 2009, *CAWCR Res. Lett.* **2**, 4–11. URL: http://cawcr.gov.au/publications/researchletters.php

Timbal B, Fawcett R. 2013. A Historical Perspective on Southeastern Australian Rainfall since 1865 Using the Instrumental Record. *J. Clim.*, **26**, 1112–1129.

VBRC2010. 2009 Victorian Bushfires Royal Commission - Final report. Parliament of Victoria, ISBN 978-0-9807408-1-3.

Vincent CL, Hahmann AN, Kelly MC. 2012. Idealised mesoscale model simulations of open cellular convection over the sea. *Bound.-Lay. Meteorol*. **142**, 103–121, doi:10.1007/s10546-011-9664-7.

Weckwerth TM, Horst TW, Wilson JW. 1999. An observational study of the evolution of horizontal convective rolls. *Mon. Weather Rev*. **127**, 2160–2179.

Weckwerth TM, Wilson JW, Wakimoto RM, Crook NA. 1997. Horizontal convective rolls: Determining the environmental conditions supporting their existence and characteristics. *Mon. Weather Rev.* **125**, 505–526.

Weckwerth TM. 2000. The effect of small-scale moisture variability on thunderstorm initiation. *Mon. Weather Rev.* **128**, 4017–4030.

Wilson JW, Foote GB, Crook NA, Fankhauser JC, Wade CG, Tuttle JD, Mueller CK. 1992. The role of boundary-layer convergence zones and horizontal rolls in the initiation of thunderstorms: A case study. *Mon. Weather Rev*. **120**, 1785–1815.

Worthington RM. 2002. Mountain waves launched by convective activity within the boundary layer above mountains. *Bound.-Lay. Meteorol*. **103**, 469–491.

Young GS, Kristovich DAR, Hjelmfelt MR, Foster RC. 2002. Rolls, streets, waves, and more. *B. Am. Meteorol. Soc*. **83**, 54–69.

Zhang JA, Katsaros KB, Black PG, Lehner S, French JR, Drennan WM. 2008. Effects of roll vortices on turbulent fluxes in the hurricane boundary layer. *Bound.-Lay. Meteorol*. **128**, 173–189, doi:10.1007/ s10546-008-9281-2.

BoM/BCRC peer-reviewed publications

Fawcett, R.J.B., W. Thurston, J.D. Kepert and K.J. Tory (2012a) Modelling the fire weather of Black Saturday. Extended abstracts, Annual Conference of the Australasian Fire and Emergency Services Council and the Bushfire Cooperative Research Centre, Perth, August 28 to 30.

Fawcett, R.J.B., W. Thurston, J.D. Kepert and K.J. Tory (2013b) Modelling the fire weather of the Eyre Peninsula fire of January 2005. Extended abstracts, Annual Conference of the Australasian Fire and Emergency Services Council and the Bushfire Cooperative Research Centre, Melbourne, September 2 to 5. In review.

Fawcett, R.J.B., A J Wain, W. Thurston, J.D. Kepert and K.J. Tory (2013e) The Melbourne dust storm revisited: an ACCESS case study. 20th International Congress on Modelling and Simulation, Adelaide, December 1 - 6.

Fawcett, R.J.B., M Webb, W. Thurston, J.D. Kepert and K.J. Tory (2013f) Modelling the fire weather of the Dunalley fire of January 2013. 20th International Congress on Modelling and Simulation, Adelaide, December 1 - 6.

Kepert, J.D., (2011) Weather Forecasting: A long way since Tropical Cyclone Tracy, Invited presentation. Extended Abstracts, Annual Conference of the Australasian Fire and Emergency Services Council and the Bushfire Cooperative Research Centre, Sydney, August 29 to 31.

Kepert, J.D., A. Wain and K.J. Tory (2012b) A comprehensive, nationally consistent climatology of fire weather parameters. Extended abstracts, Annual Conference of the Australasian Fire and Emergency Services Council and the Bushfire Cooperative Research Centre, Perth, August 28 to 30.

Kepert, J.D., R.J.B. Fawcett, W. Thurston and K.J. Tory (2013) Applications of very high resolution atmospheric modelling for bushfires. Extended abstracts, Annual Conference of the

Australasian Fire and Emergency Services Council and the Bushfire Cooperative Research Centre, Melbourne, September 2 to 5. In preparation.

Kepert, J.D. and R.J.B. Fawcett (2013a) Meteorological aspects of the Margaret River fires on November 2011. Extended abstracts, 20th International Congress on Modelling and Simulation, Adelaide, December 1 - 6.

Thurston, W., R.J.B. Fawcett, K.J. Tory and J.D. Kepert (2013a) Simulating boundary-layer rolls with a numerical weather prediction model. *For submission to Q. J. Royal Meteorol. Soc.*

Thurston, W., K.J. Tory, R.J.B. Fawcett and J.D. Kepert (2013b) Large-eddy simulations of bushfire plumes in the turbulent atmospheric boundary layer. 20th International Congress on Modelling and Simulation, Adelaide, December 1 - 6.

BoM/BCRC Internal-reviewed publications

Fawcett, R.J.B., W. Thurston, J.D. Kepert and K.J. Tory (2012b). Modelling the fire weather of the Eyre Peninsula fire of January 2005. Poster, Annual Conference of the Australasian Fire and Emergency Services Council and the Bushfire Cooperative Research Centre, Perth, August 28 to 30.

Fawcett, R.J.B., W. Thurston, J.D. Kepert and K.J. Tory (2012c) Blue Mountains case study – December 2001. Project report to the Bushfire CRC.

Fawcett, R.J.B., W. Thurston, J.D. Kepert and K.J. Tory (2012d) Blue Mountains case study – December 2001. Additional material. Project report to the Bushfire CRC.

Fawcett, R.J.B., W. Thurston, J.D. Kepert and K.J. Tory (2013a) The meteorology of Black Saturday: a high-resolution ACCESS modelling study. CAWCR Technical Reports, in review.

Fawcett, R.J.B., W. Thurston, J.D. Kepert and K.J. Tory (2013c) Modelling the fire weather of the Coonabarabran fire of 13 January 2013. Poster, Annual Conference of the Australasian Fire and Emergency Services Council and the Bushfire Cooperative Research Centre, Melbourne, September 2 to 5. Submitted.

Fawcett, R.J.B., W. Thurston, J.D. Kepert and K.J. Tory (2013d) Modelling the Weather on Black Saturday. Poster, Australian Meteorological and Oceanographic Society, Melbourne, February 11 to 13.

Fawcett, R.J.B., M Webb, W. Thurston, J.D. Kepert and K.J. Tory (2013g) Modelling the fire weather of the Dunalley fire of January 2013. Papers presented at the Science to Services Workshop, Bureau of Meteorology, Melbourne, August 15 - 16. Submitted.

Kepert, J.D., L.W. Logan and K.J. Tory (2011a) Modelling the fire weather on Black Saturday, Poster, Annual Conference of the Australasian Fire and Emergency Services Council and the Bushfire Cooperative Research Centre, Sydney, August 29 to 31.

Kepert J.D., P.J. Steinle, C.I.W. Tingwell and K.J. Tory (2011b) Verification of High-Resolution Forecasts from ACCESS. Poster, Annual Conference of the Australasian Fire and Emergency Services Council and the Bushfire Cooperative Research Centre, Sydney, August 29 to 31.

Kepert J.D. and K.J. Tory (2011c) Using Numerical Weather Prediction to Forecast Wind Direction Variability. Poster, Annual Conference of the Australasian Fire and Emergency Services Council and the Bushfire Cooperative Research Centre, Sydney, August 29 to 31.

Kepert, J.D., R.J.B. Fawcett and M. Peace (2012a) Meteorological Aspects of the Margaret River Fires on 23 November 2011. Poster, Annual Conference of the Australasian Fire and Emergency Services Council and the Bushfire Cooperative Research Centre, Perth, August 28 to 30.

Kepert, J.D. and R.J.B. Fawcett (2013b) Meteorological aspects of the Margaret River fires on November 2011. Poster, Australian Meteorological and Oceanographic Society, Melbourne, February 11 to 13.

Thurston, W. (2012a) Updraft phenomena in wildfires: an annotated bibliography. Project report to the Bushfire CRC.

Thurston, W., R.J.B. Fawcett, J.D. Kepert and K.J. Tory (2012b) Forecasting wind direction variability using numerical weather prediction. Poster, Annual Conference of the Australasian Fire and

Emergency Services Council and the Bushfire Cooperative Research Centre, Perth, August 28 to 30.

Thurston, W., R.J.B. Fawcett, J.D. Kepert and K.J. Tory (2012c) Idealised numerical modelling of bushfire plumes. Poster, Annual Conference of the Australasian Fire and Emergency Services Council and the Bushfire Cooperative Research Centre, Perth, August 28 to 30.

Thurston, W., J.D. Kepert, R.J.B. Fawcett and K.J. Tory (2012d) A note on the ACCESS configuration used to investigate wind variability and boundary-layer structure. Project report to the Bushfire CRC.

Thurston, W., K.J. Tory and J.D. Kepert (2012e) Briefing note: choice of updraft phenomena conducive to firebrand lofting. Project report to the Bushfire CRC.

Thurston, W., K.J. Tory, J.D. Kepert and R.J.B. Fawcett (2013c) *Briefing note: model configuration for investigating updraft phenomenon number one.* Project report to the Bushfire CRC.

Thurston, W., K.J. Tory, J.D. Kepert and R.J.B. Fawcett (2013d) *Briefing note: model configuration for investigating updraft phenomenon number two.* Project report to the Bushfire CRC.

Thurston W, Fawcett R, Tory K and Kepert J 2012. *Idealised numerical modelling of bushfire plumes*. Conference poster, Annual Conference of the Australasian Fire and Emergency Services Council and the Bushfire Cooperative Research Centre, Perth, 28 to 30 August 2012.

Thurston W, Fawcett R, Tory K and Kepert J 2012. *Forecasting wind direction variability using numerical weather prediction.* Conference poster, Annual Conference of the Australasian Fire and Emergency Services Council and the Bushfire Cooperative Research Centre, Perth, 28 to 30 August 2012.

Thurston W, Tory K, Fawcett R and Kepert J 2013. *Idealised numerical modelling of bushfire plumes*. Conference presentation, Annual Conference of the Australian Meteorological and Oceanographic Society, Melbourne, 11 to 13 February 2013

Thurston W, Tory K J, Fawcett R J B and Kepert J D 2013. *Idealised numerical modelling of bushfire plumes and their potential for firebrand lofting*. Conference Poster. Annual Conference of the Australasian Fire and Emergency Services Council and the Bushfire Cooperative Research Centre, Melbourne, 2 to 5 September 2013

Thurston W, Tory K J, Fawcett R J B and Kepert J D 2013. *Large-eddy simulations of bushfire plumes in the turbulent atmospheric boundary layer*. Conference Poster. Annual Conference of the Australasian Fire and Emergency Services Council and the Bushfire Cooperative Research Centre, Melbourne, 2 to 5 September 2013.

Thurston W (2013). *Large-eddy simulations of bushfire plumes in the turbulent atmospheric boundary layer*. Invited conference presentation, 2013 CSIRO Bushfire behaviour science symposium, Canberra, 14-16 October 2013.

Thurston W, Tory K J, Fawcett R J and Kepert J D 2013. *Large eddy simulations of bushfire plumes in the turbulent atmospheric boundary layer*. Conference presentation, The Tenth Symposium on Fire and Forest Meteorology, American Meteorological Society, Bowling Green, Kentucky, USA, 15 to 17 October.

Thurston W, Tory K J, Fawcett R J B and Kepert J D 2013. *Large-eddy simulations of bushfire plumes in the turbulent atmospheric boundary layer*. Conference presentation, 20th International Congress on Modelling and Simulation, Adelaide, 1 to 6 December 2013.

Tory K J, Thurston W, Fawcett R J and Kepert J D 2013. *Boundary-layer rolls and their potential impact on bushfires: a high resolution NWP case study*. Conference presentation. The Tenth Symposium on Fire and Forest Meteorology, American Meteorological Society, Bowling Green, Kentucky, USA, 15 to 17 October 2013.